# Shear-wave Seismic Study above Vigindustries, Inc. Legacy Salt Jugs in Hutchinson, Kansas

Richard D. Miller, Julian Ivanov, Steven D. Sloan, Shelby L. Walters,
Birgit Leitner,* Arno Rech,* Brett A. Wedel, Anthony R. Wedel, Joe M. Anderson,
Owen M. Metheny, and Justin C. Schwarzer

Kansas Geological Survey
1930 Constant Avenue
Lawrence, Kansas 66047

**Final Report to**

**William T. Shefchik**
**Burns & McDonnell Engineering Company**
**9400 Ward Parkway**
**Kansas City, MO 64114**

Compiled and formatted by Mary Brohammer
*Students from University of Leoben, Austria

**Open-file Report No. 2009-3**

**March 2009**

# Shear-wave Seismic Study above Vigindustries, Inc. Legacy Salt Jugs in Hutchinson, Kansas

by

Richard D. Miller
Steven D. Sloan
Shelby L. Walters
Julian Ivanov
Birgit Leitner*
Arno Rech*
Brett A. Wedel
Anthony R. Wedel
Joe M. Anderson
Owen M. Metheny
Justin C. Schwarzer

Kansas Geological Survey
1930 Constant Avenue
Lawrence, Kansas 66047

final report to

William T. Shefchik
Burns & McDonnell Engineering Company
9400 Ward Parkway
Kansas City, MO 64114

March 2009

KGS Open-file Report 2009-3

Compiled and formatted by Mary Brohammer
*Students from University of Leoben, Austria

# Shear-wave Seismic Study above Vigindustries, Inc. Legacy Salt Jugs in Hutchinson, Kansas

## Table of Acronyms

| | |
|---|---|
| CDP | Common depth point |
| CMP | Common mid point |
| DC | Direct current |
| DGPS rtk | Differential global positioning system with real-time kinematic |
| MASW | Multichannel analysis of surface waves |
| NMO | Normal moveout |
| PC | Personal computer |
| QA/QC | Quality assurance/quality control |
| SASW | Spectral analysis of surface waves |
| S/N | Signal-to-noise ratio |
| VSP | Vertical seismic profile |
| ZVSP | Zero-offset vertical seismic profile;<br>near-vertical offset vertical seismic profile |

# Shear-wave Seismic Study above Vigindustries, Inc. Legacy Salt Jugs in Hutchinson, Kansas


**Executive Summary**

This applied research project correlated measured shear-wave velocities with the condition of dissolution voids and the physical properties of the overburden. Shear-wave velocities were estimated using seismic-reflection and MASW data acquired along eight profiles that intersected four representative dissolution wells, two with voids isolated to the salt interval and two with voids that had migrated into the shale. These four wells were recently re-entered and tested to appraise the void geometry, determine the configuration and location of the roof, and estimate the integrity of the overlying strata. Horizontally polarized shear-wave reflection profiling was used to map reflections from and above the top of salt and measure the normal moveout velocity (NMO) of the material between each reflector and the ground surface. A downhole velocity survey was used to produce predictive models and establish ground truth for the shear-wave reflection data. Elevated shear-wave velocities correlate to areas where voids are known to have breached the shale/salt contact at around 400 ft below ground surface, but not moved beyond the "three-finger" dolomite. Decreased shear-wave velocity is measured at sites where voids have migrated to the ground surface forming sinkholes and sites where voids are well below the top of salt.

Eight fixed-spread CMP profiles were acquired across four abandoned dissolution-well sites recently opened and interrogated with sonar, electric logs, and an acoustic televiewer. Two orthogonal 240-channel, 780-ft-long shear-wave profiles were acquired at each well site with the intersection of the two lines as near the well location as possible. Shear-wave reflections from the bedrock, "three finger" dolomite, and the top of Hutchinson Salt Member can all be confidently identified. The short, focused spreads result in a reduced subsurface coverage with increasing depth, and therefore the spatial sampling at the salt/shale contact is less than 50 ft on most lines.

With shear-wave velocity being a function of shear modulus and density, changes in stress of overburden rocks prior to strain will result in changes in shear velocity. Therefore, the observed local increases in shear velocity between the "three finger" dolomite and the bedrock surface can be equated to increased stress associated with overburden roof load prior to collapse or spall of the void roof. Increases in average shear velocity between the dolomite and bedrock would be consistent with voids that have migrated out of the salt and into the shale. Relative decreases in shear velocity are related to areas where subsidence features are present at the ground surface or interpreted at the top of bedrock. The shear-wave velocity of the unconsolidated materials appears to be consistent across all the areas examined with seismic reflection. The consistent variability in the shear velocity appears to be related to void condition and location and is constrained to the interval between the top of bedrock and the "three finger" dolomite.

MASW data were acquired to investigate any relationship between changes in shear velocity along the bedrock surface and differences in the position and condition of the four invasively investigated voids. Two profiles were acquired at sites representative of a void deep in the salt and native conditions in the predominantly shale overburden and one site with a void that was measured with sonar to extend well into the shale. With the dependence of surface-wave sampling depth on frequency, generating very low frequency surface waves to sample the bedrock surface at around 60 to 70 ft was imperative. The maximum apparent sampling depth of the MASW data was around 40 ft. To evaluate the full potential of this method to scan the

bedrock surface for elevated stress and therefore risk of failure, lower frequencies must be recorded. An interesting and unexpected feature apparent on one of the two lines of MASW data can be interpreted to represent a zone within the unconsolidated sediments that may have experienced subsidence confined to the lower half of the alluvial interval. This apparent subsidence area is coincident with a low velocity and reduced S/N area on the coincident shear-wave reflection profile at the bedrock surface. Clearly, MASW has great potential for scanning the bedrock surface for zones of elevated shear velocity if lower frequencies can be produced and recorded.

In advance of the surface seismic-data acquisition, a downhole velocity survey was conducted in borehole #39. These data are a direct measure of the shear-wave velocity at this location as a function of depth and provide a direct tie to potential reflecting interfaces. Identification of reflections on shot gathers and the geometry of the survey were based on synthetic shot gathers generated using the lithologic logs and the one-way travel times from the downhole survey. The match between the seismic-reflection data and the model generated from the borehole velocity data is outstanding and provides excellent ground truth for both reflections and their apparent velocity as estimated from the NMO curves.

Change in shear-wave velocity of the shale overburden is predictable and sensitive to voids known to have migrated outside the salt at this site. Increases in shear-wave velocity within the undisturbed portion of the shale overburden are observed to be more than 15% in places where voids greater than 100 ft in diameter have migrated into the upper Wellington Shale formation but still below the "three finger" dolomite. Localized decreases in the NMO velocity between the "three finger" dolomite and the bedrock appear consistent with subsidence expressed within the unconsolidated interval. MASW could be an early indicator of areas with a relative increase in potential risk for imminent collapse. Using MASW data for this purpose would only be possible if 4- to 8-Hz surface waves could be produced and recorded, allowing full sampling of the bedrock surface.

**Introduction**

Dissolution mining of the Hutchinson Salt Member over 100+ years has left a legacy of unstable voids, some with the potential to result in sinkholes. Areas exist within the old North American Salt Company solution-mine field where the current conditions of the old jugs are unknown and therefore need to be investigated to assure public safety (Figure 1). Four old jugs and associated wells were targeted for initial investigations to develop a protocol for investigation and to establish a potential range of jug conditions. Two wells were selected with good records and were suspected to be in good, stable condition. Two other wells with a relatively higher probability of instability were also picked for study. The set of criteria used to make the selections really had no bearing on the seismic investigation, but included age, amount of salt left above the jug based on plugging records, proximity to property boundaries, etc.

Borehole studies at the sample-well sites included borehole logs (electric and lithologic), sonar of the void areas, and acoustic televiewer. These data provided excellent information about the current condition of the voids and the characteristics of the near-borehole materials. Key to the overall characterization objectives at this site is determining which old jugs should be classified as high priority on the remediation lists. Geophysics represents the only possible site-wide approach to characterizing the static condition of these wells prior to drilling out the well plugs. Of the various surface geophysical approaches that have some potential for detecting these voids, seismic has the necessary theoretical resolution and sensitivity to be successful. Specifically looking for areas with vertical migration potential and with previous experience at

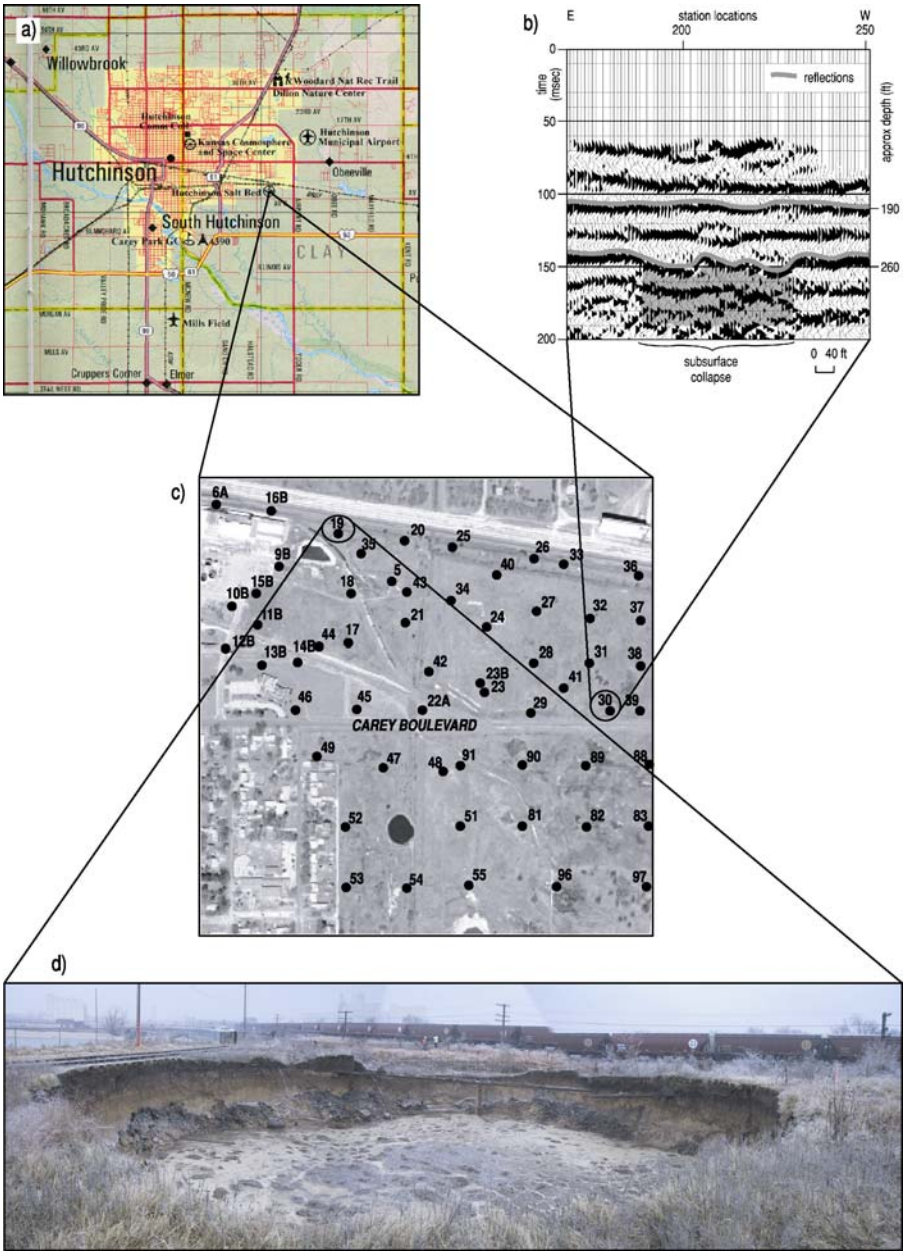


Figure 1. Site map showing a) location of the sinkhole in relation to the city of Hutchinson, b) seismic data from a sinkhole investigated, c) an orthomap of the area affected by the sinkhole, and d) a photo of the sinkhole after subsidence on January 7, 2005.

this site, shear-wave velocity measurements could provide the information necessary to predict different levels of stress on any unsupported span of roof rock associated with migrating voids.

Historical use of high-resolution seismic reflection to image the internal geometries and overburden characteristics associated with salt dissolution have met with varying degrees of success. Previous attempts to image the salt and overlying Permian strata have used compressional-wave energy. Considering the various targets and objectives, compressional-wave surveys have been the ideal choice.

**Previous High-Resolution Compressional-Wave Seismic-Reflection Studies at Sinkhole Sites**

High-resolution seismic-reflection surveys targeting the Hutchinson Salt Member have collectively provided critical insights and valuable site-specific characteristics of subsidence features throughout Kansas. Significant findings from these various studies are collectively applicable to any region underlain by massive bedded salt layers and in general to any collapse processes in a subsidence-prone setting. A high concentration of seismic profiles has been collected along the natural dissolution front and specific dissolution mine fields where subsidence has threatened transportation and/or population centers. This concentrated area of study in conjunction with several sinkhole investigations scattered around the central part of the state of Kansas allow empirical development of mechanisms and settings controlling and influencing the subsidence process (Figure 2).

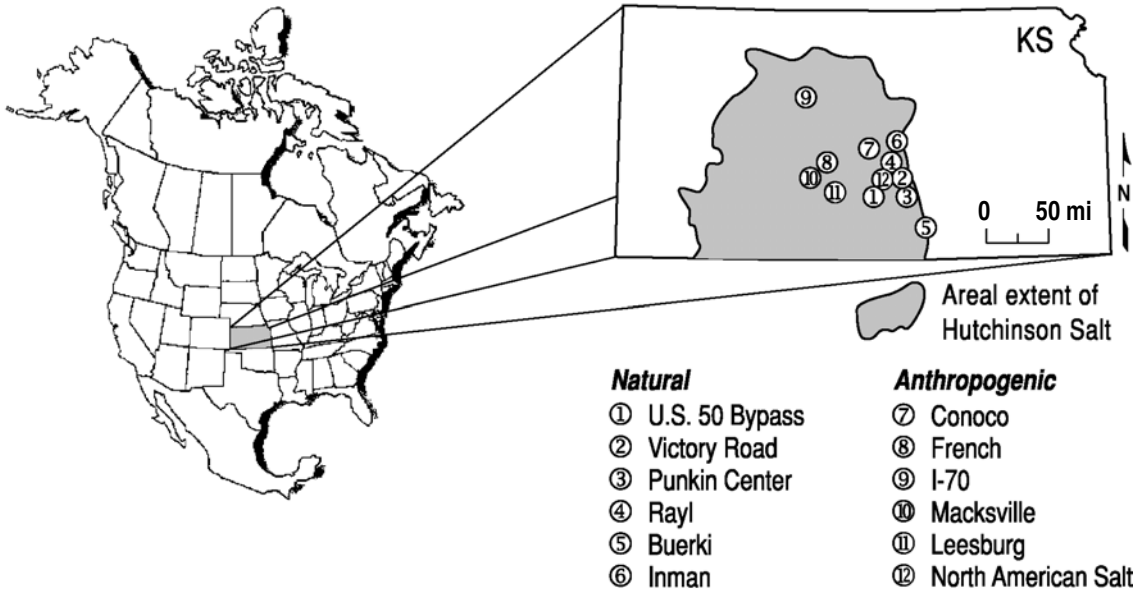


Figure 2. Map of Kansas with outline of areal extent of Hutchinson Salt Member. Numerically identified on the map are locations of 12 high-resolution seismic-reflection surveys targeting individual sinkholes. These sites include approximately 40 mi of high-resolution seismic data on 28 different lines, all acquired, processed, and interpreted by KGS.

A range of sinkhole types and locations has been seismically investigated en route to addressing site-specific questions generally related to prediction of future growth rates and affected surface. In part, as a consequence of these focused studies, the high-resolution seismic-reflection method has been refined and, therefore, evolved over the last 15 years to more effectively and accurately image extreme structural anomalies. Sinkholes included in these various studies have formed as a result of salt dissolution both in proximity to well bores (dissolution mining, brine disposal, oil wells, seismic shot holes, etc.) and in areas known to experience natural dissolution with no apparent anthropogenic influences. The eastern boundary of the salt is a natural leaching environment where sinkholes have been forming for millions of years and is significantly less predictable and potentially controllable than subsidence resulting from anthropogenic fluid sources.

Hydrology is the component of dissolution-instigated subsidence that most significantly distinguishes anthropogenic from natural processes. With the fluid-access points (inlet and exit)

fixed for the anthropogenic-induced dissolution case, the process is clearly constrained to a volume of salt commensurate with the dynamics of the fluid and available salt stock. Although in general the processes are identical, resulting structures, fluid volumes/velocities, and time frames are dramatically different.

***Investigations at this Site***

A sinkhole that catastrophically formed near a city street and railroad spur in the early 1990s at this site prompted the acquisition of a 750-ft seismic-reflection profile adjacent to the sinkhole intersecting both the road and railroad spur (Figure 3; Miller et al., 1993). That applied research project was designed to determine the capabilities of shallow seismic reflection in appraising the subsurface condition around the small sinkhole near Carey Boulevard (Figure 1). The results of that study provided a detailed look at the distortion in rock layers overlying a salt jug, where evidence of the upward progression of subsurface failure and collapse were prominent. By extrapolating the subsurface expression (as evidenced by highly disturbed reflections) upwards to the ground surface, ground movement was suggested to occur more than 150 ft away from the 1991 sinkhole expression sometime in the future. Drilling confirmed the subsidence observed on seismic within the Permian shale.

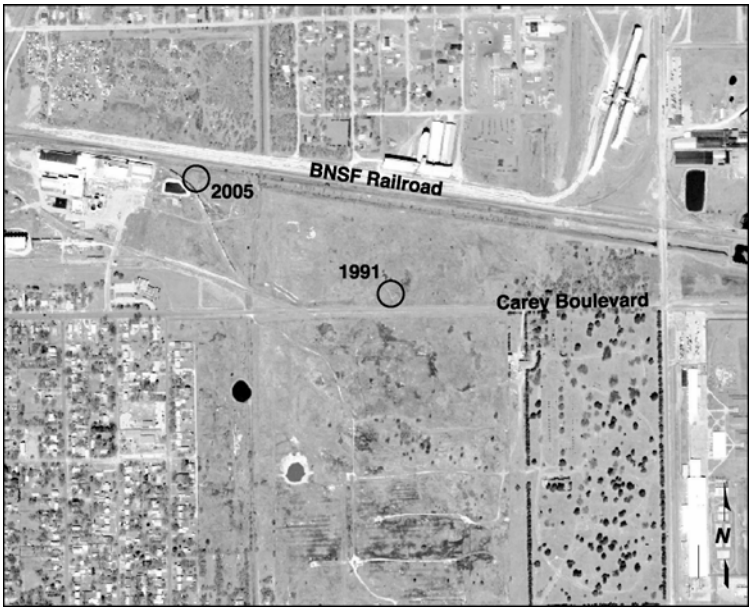

Figure 3. Site map showing nearby areas where previous seismic-reflection studies have taken place.

A second seismic-reflection survey at this site was commissioned when concerns arose for public safety and property due to a sinkhole that formed catastrophically in 2005 within 120 ft of a heavily traveled east/west railroad main line (Figure 3). A continuous CMP seismic-reflection profile approximately 600 ft long was centered on the well #19 sinkhole and approximately half way between the north edge of the sinkhole and the southernmost set of railroad tracks (Figure 4). These data were acquired under significant site-access restrictions, mainly related to physical limitations of working in a railroad drainage ditch along an active subsidence feature on one side and railroad yard on the other.

These past two seismic-reflection surveys at this site were designed to delineate the subsurface expression of existing sinkholes and to estimate future expansion. No studies had previously been attempted where the objective was to acquire seismic information that would allow predictions to be made as to an individual void's relative potential (in comparison to all voids in the field) to migrate to the bedrock surface. Estimates of that sort required the measurement of overburden-material strength characteristics and estimates of stress build-up in the roof rocks.

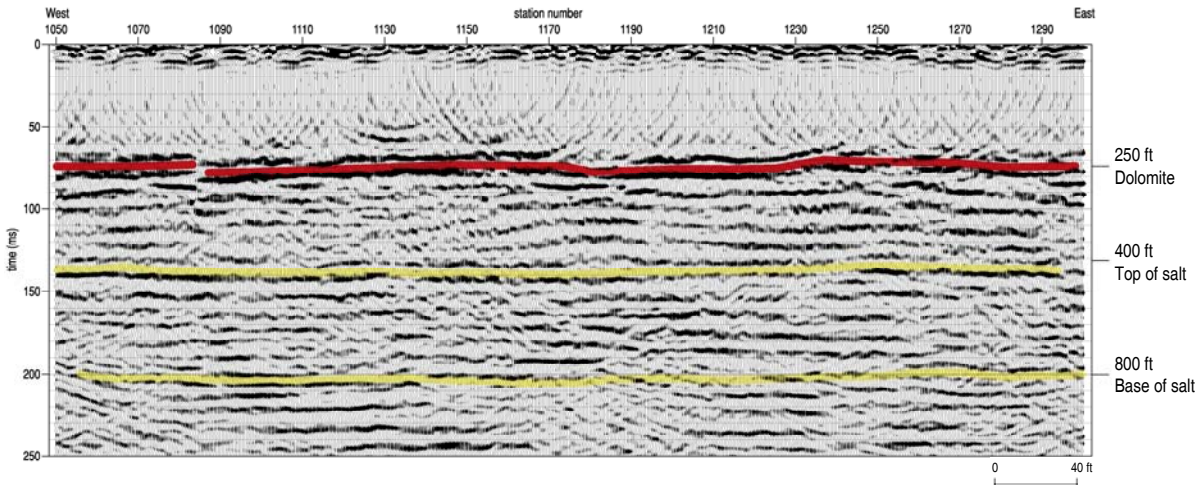


Figure 4. CMP stacked section immediately north of well #19 sinkhole.

## Site Characteristics

### *Geologic and Geophysical Setting*

The Permian Hutchinson Salt Member occurs in central Kansas, northwestern Oklahoma, and the northeastern portion of the Texas Panhandle, and is prone to and has an extensive history of dissolution and formation of sinkholes (Figure 5). In Kansas, the Hutchinson Salt Member possesses an average net thickness of 250 ft and reaches a maximum of over 500 ft in the southern part of the basin (Figure 2). Deposition occurring during fluctuating sea levels caused numerous halite beds, 0.5 to 10 ft thick, to be formed interbedded with shale, minor anhydrite, and dolomite/magnesite. Individual salt beds may be continuous for only a few miles despite the remarkable lateral continuity of the salt as a whole (Walters, 1978).

The distribution and stratigraphy of the salt is well documented (Dellwig, 1963; Holdoway, 1978; Kulstad, 1959; Merriam, 1963). The salt reaches a maximum thickness in central Oklahoma and thins to depositional edges on the north and west, erosional subcrop on the east, and facies changes on the south. The increasing thickness toward the center of the salt bed is due to a combination of increased salt and more and thicker interbedded anhydrites. The Stone Corral Formation (a well documented seismic marker bed) overlies the salt throughout Kansas (McGuire and Miller, 1989). Directly above the salt at this site is a thick sequence of Permian shales.

The upper 2500 ft of rock at this site is Permian shales (Merriam, 1963). The Chase Group (top at 1000 ft deep), lower Wellington Shales (top at 800 ft deep), Hutchinson Salt (top at 400 ft deep), upper Wellington Shales (top at 240 ft deep), and Ninnescah Shale (top at 75 ft deep) make up the packets of

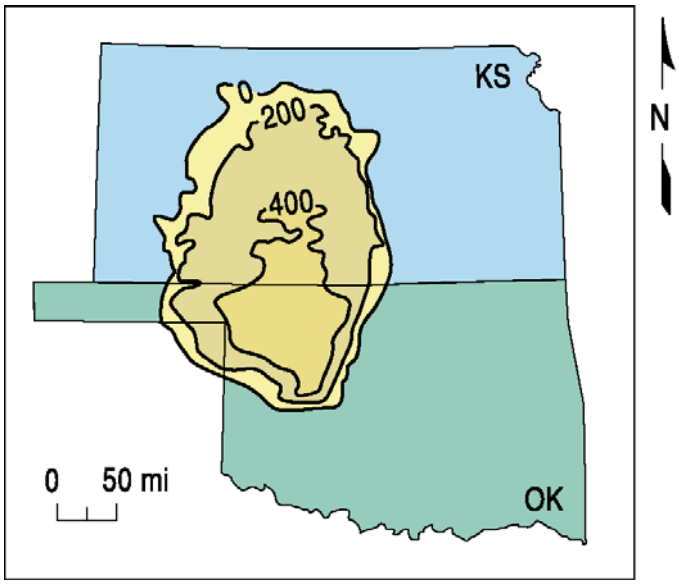


Figure 5. Approximate extent of salt formation, with contour intervals expressed in feet.

reflecting events easily identifiable and segregated within the Permian portion of the section (Figure 6). Bedrock is defined as the top of the Ninnescah Shale with the unconsolidated Pliocene-Pleistocene Equus beds making up the majority of the upper 100 ft of sediment. Thickness of Quaternary alluvium that fills the stream valleys and paleosubsidence features goes from 0 to as much as 300 ft, depending on the dimensions of the features.

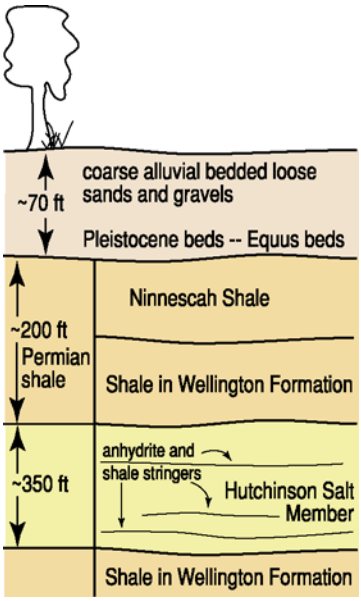

Figure 6. Generalized geology.

Recent dissolution of the salt and resulting subsidence of overlying sediments forming sinkholes has generally been associated with mining or saltwater disposal (Walters, 1978). Historically, these sinkholes can manifest themselves as a risk to surface infrastructure. The rate of surface subsidence can range from gradual to catastrophic. Besides risks to surface structures, subsidence features potentially jeopardize the natural segregation of ground-water aquifers, greatly increasing their potential to negatively impact the environment (Whittemore, 1989, 1990). Natural sinkholes resulting from dissolution of the salt by localized leaching within natural flow systems which have been altered by structural features (such as faults and fractures) are not uncommon west of the main dissolution edge (Merriam and Mann, 1957).

Caprock and its characteristics are a very important component of any discussion concerning dissolution, subsidence, and formation of sinkholes. The Permian shales (Wellington and Ninnescah) that overlay the Hutchinson Salt Member are about 200 ft thick in this area and are characterized as generally unstable when exposed to freshwater, being susceptible to sloughing and collapse (Swineford, 1955). These Permian shales tend to be red or reddish-brown and are commonly referred to as "red beds." Permian red beds are extremely impermeable to water and have therefore provided an excellent seal between the freshwaters of the Equus beds and the extremely water-soluble Hutchinson Salt Member. The modern-day expanse and mere presence of the Hutchinson Salt is due to the protection from freshwater provided by these red beds.

Isolating the basal contact of the Wellington Formation provides key insights into the general strength of roof rock expected if dissolution-mined salt jugs (salt jugs are the cavities or voids, many times shaped like jugs, in the salt that form after salt has been dissolution mined in proximity to the wells) reach the top of the salt zone. Directly above the salt/shale contact is an approximately 20-ft-thick dark-colored shale with joint and bedding cracks filled with red halite (Walters, 1978). Once unsaturated brine comes in contact with this shale layer, these red-halite-filled joints and bedding planes are rapidly leached, leaving an extremely structurally weak layer.

***Dissolution Mining and Subsidence***

Subsidence resulting in sinkholes within dissolution mine fields in and around the city of Hutchinson, Kansas have been reported for over ninety years (Walters, 1978). Mining of the Hutchinson Salt Member has generally involved one of three different techniques: single well, multi-well, and room-and-pillar. Sinkholes related to solution mining of the Hutchinson Salt Member to date have formed as a result of roof failure associated with the single-well mining method. In general, the single-well method involves injecting freshwater near the base of the salt and recovering the brine solution near the top of the salt, all through the same multi-plumbed borehole (Figure 7).

Problems with the single-hole method begin to occur as the volume of salt removed below shale or anhydrite stringers within the salt reaches a point where the unsupported span of these interbedded non-soluble layers exceeds a distance its strength will endure (Figure 8a). Failure of these beds in proximity to the well bore generally results in rupture of the freshwater tubing and upward movement of the dissolution zone (Figures 8b). Once the failure and collapse cycle reaches the shale caprock, the process becomes much more horizontal (Figure 8c). Eventually this lateral movement of the dissolution front may, in some cases, contact an equivalent void developing from an adjacent well, forming what is called a gallery (Figure 9).

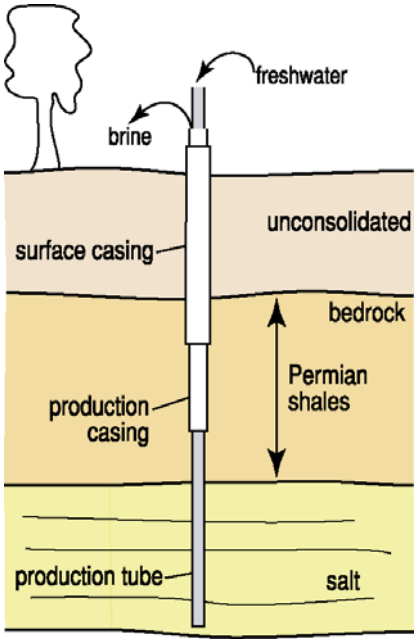


Figure 7. Illustration of general installation design of single-well facilities in the Hutchinson, Kansas, area.

With the abundance of locally continuous but regionally discontinuous insoluble beds within the Hutchinson Salt Member in Kansas (Walters, 1978), vertical growth of a dissolution volume within the salt will be constrained and guided by these interbedded, insoluble confining surfaces. From initial dissolution near the water inlet until vertical growth of a void results in contact with an insoluble layer, the geometry of the cavern is controlled by the differential gravity of the fluids, the location of inlet and drain, and velocity and volume of fluids moving through the inlet and drain. The pattern of void growth can be very complex and progress at irregular rates throughout the growth cycle.

With the greater density of brine relative to water, active dissolution zones in salt will tend to migrate upward or outward along the base of an insoluble upper confining layer. Voids originating near the top of the salt will generally manifest themselves as relatively thinner,

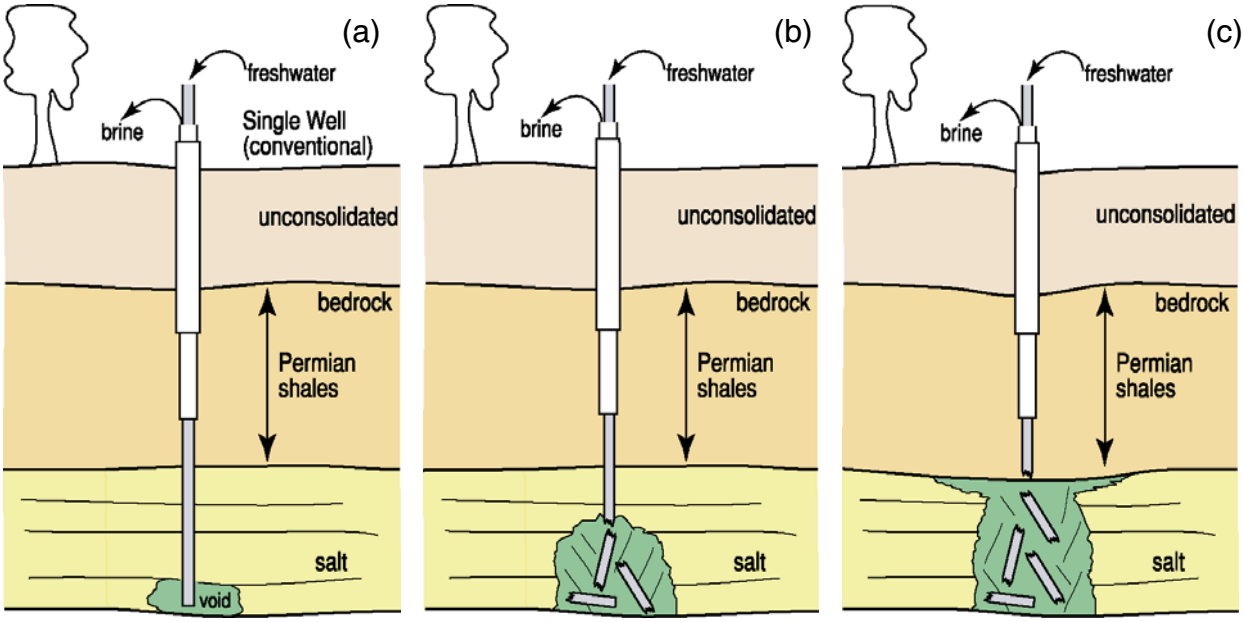


Figure 8. Historic progress of single-well solution mining from base of salt (a) through overproduction (c) and development of morning-glory structure at the top of salt.

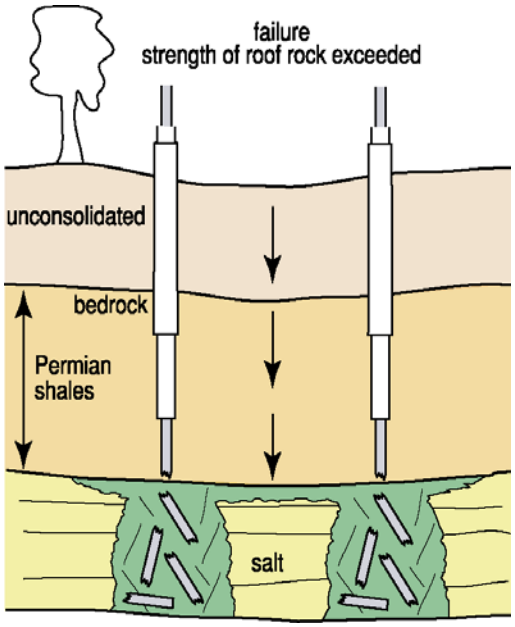


Figure 9. Inadvertent formation of a gallery from the joining of two morning-glory structures from adjacent wells and resulting sag.

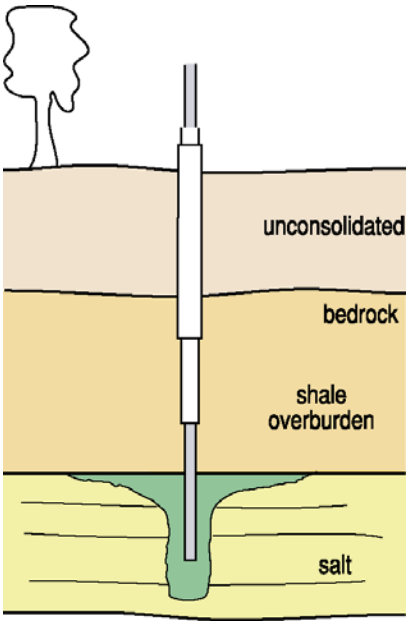


Figure 10. Illustration of morning-glory structure that can result from historical mining methods. Unsupported roof span exceeds design maximums and relative risk of failure is increased.

more lenticular features with a larger surface area relative to volume in comparison to voids originating deeper in the salt interval. Voids originating deeper in the salt interval will preferentially grow upward, elongating vertically until an insoluble interbed arrests growth. This process is clearly evident in some pre-1975 salt jugs where the diameters of the tops of the jugs were enlarged to form a morning-glory geometry (Figure 10) (Landes and Piper, 1972). Caverns mined after new regulations came into effect in 1975 have thick salt roofs, so they do not have the morning-glory shape.

When caprock fails, vertical growth continues progressively upward layer by layer through the overburden as stress exceeds the strength in each successive unsupported span of new roof rock. Maximum potential strain is limited by the void height. The void space available within the salt interval to accommodate roof-collapse material is the key characteristic determining whether void movement through the entire overburden-rock column proceeds as a rapid continuous process or it progresses as intermittent segments. However, ground-water-flow patterns that prevailed during solution mining were altered within the salt interval and affected by overburden lag with each subsequent subsidence event, effectively changing the dynamics of salt harvesting.

The fall of roof rock instigated by the growth of active dissolution voids changed the hydrologic properties of the system and therefore the leaching rate and location within the salt. Changes in the leaching rate during mining can range from a complete halt to a minor alteration in fluid-flow patterns, thereby directly affecting the dissolution activity along the front. Dramatic changes in fluid-flow characteristics, especially as a result of blockages or restrictions at the inlet and/or drain from collapsed roof rock during mining, are the most likely scenarios responsible for halting the dissolution process at a specific location.

**Stress Relationship to Seismic Properties**

Changes in the shear-wave velocity are a key indicator of either previous subsidence activity or areas were voids have a strong potential for roof collapse. Shear-wave velocities of materials are estimated from material responses to stress and strain. Because failure of consolidated rock is related more to the matrix than the pore conditions, monitoring changes in the shear-wave velocity should represent a highly sensitive method of detecting load related changes in stress. Changes in shear velocity for a particular rock are related to differential stress and associate non-linearity in the stress/strain curve (Dvorkin et al., 1996).

The shear-wave velocity is defined as

$$Vs = \{\mu/\rho\}^{1/2},$$

where $\mu$ is the shear modulus and $\rho$ is the bulk density. With bulk density considered constant (assuming no change in pore fluids), the shear modulus controls the shear-wave velocity of a rock. The shear modulus is defined as the ratio of force per unit area divided by the associated change in lateral cross section for a given length (Figure 11). Shear modulus and Young's Modulus are considered constant for a material under static pressures and within the elastic-deformation portion of the stress/strain curve (Figure 12).

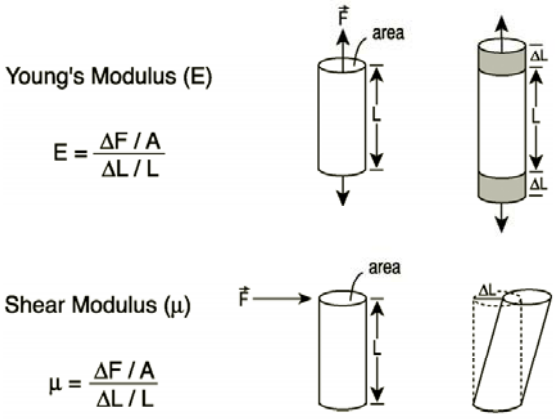


Figure 11. Elastic moduli that control seismic velocity in rocks.

Laboratory measurements of compressional and shear-wave velocities show marked, non-linear increases with increased confining stress (Khaksar et al., 1999). These measured changes in velocity of samples suggest variations in effective stress, like those present above a void with a large roof span or a reservoir under production pressures, could cause significant changes in velocity of the affected rocks. Carrying the confining stress to the logical extreme introduces plastic deformation and rupture (Figure 12). At this end of the stress/strain curve, strain response over a small range of stress is substantial. Shear velocity is reduced when mechanical damage occurs in the rock as a result of stress-induced plastic deformation (Winkler, 2005).

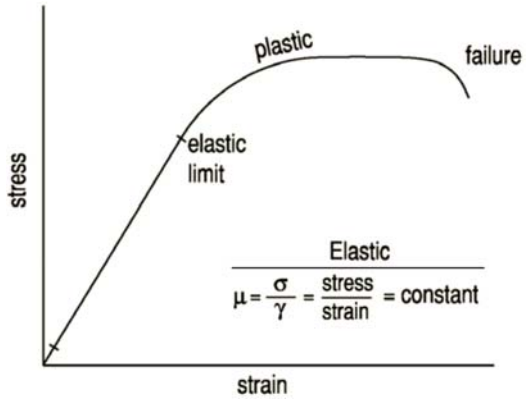


Figure 12. Stress/strain relationship for ideal material.

Key indicators of either subsidence activity or areas with a strong potential for roof collapse are lateral decreases in the shear-wave velocity related to compaction changes (Figure 13) and localized increases in shear-wave velocity associated with the tension dome surrounding subsurface cavities (Figure 14). When gradual subsidence is or has been active, a notable, localized drop in shear-wave velocity is characteristic of earth materials that have undergone sufficient strain to be characterized within the plastic-deformation portion of the stress/strain curve. When stoping or overburden drape has fallen into voids, the reduced compaction zone—which starts at the void and moves generally vertically toward the surface—will produce a

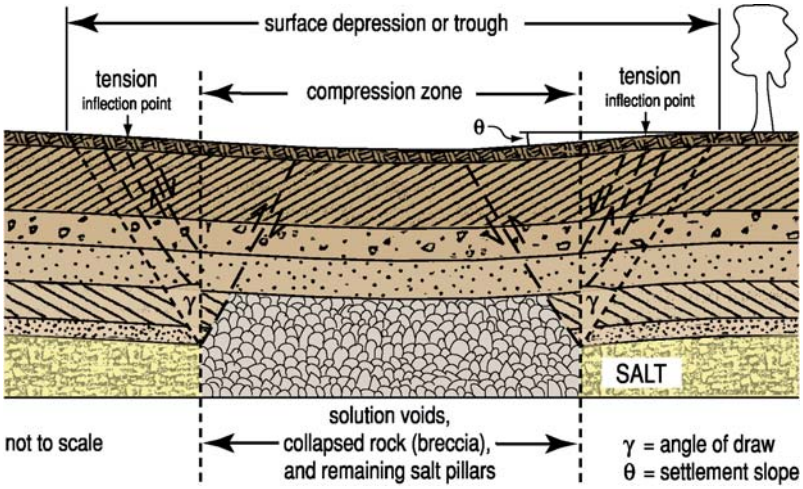


Figure 13. Cross section of the anatomy of a subsidence trough showing angle of draw, compression zone, tension zone, and inflection points for a sag feature.

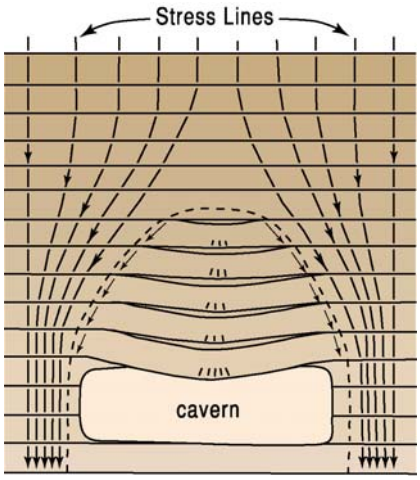


Figure 14. Tension dome and distribution of stress lines around a cavern opening in horizontal strata (modified from Davies, 1951).

characteristic signature in the shear-wave velocity field consistent with its subsidence pattern. Confidently mapping the subsidence geometry depends on abruptness of the contrast (gradient) between the disturbed and undisturbed earth materials, the geometry, dimensions, and depth of the anomaly, and characteristics of seismic-source energy.

The strength of individual rock layers can be qualitatively described in terms of stiffness/rigidity and empirically estimated from measurements of the shear-wave velocity. Shear-wave velocity is directly proportional to stress and inversely related to strain. Because the shear-wave velocity of earth materials changes when the stress on those materials becomes "large," it is reasonable to suggest load-bearing roof rock above mines or dissolution voids may experience elevated shear-wave velocities due to loading between pillars, or, in the case of voids, loading between supporting side walls (Figure 15). This localized increase in shear velocity is not related to increased strength, but quite the contrary, to increased load. High-velocity shear-wave "haloes" encompassing low-velocity anomalies are key indicators of an increased relative potential for near-term roof failure.

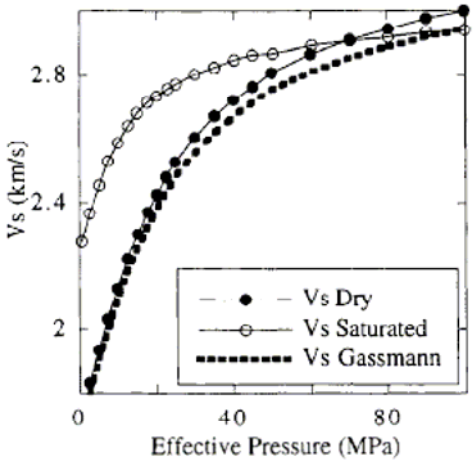


Figure 15. Shear wave velocity change with increased confining pressures (after Coyner, 1984).

**Program Objectives and Work Plan**

Ranking of abandoned salt jugs for relative risk based on the need for remediation calls for a characterization program with a quantitative method for assigning priorities to each well bore and associated jug of interest. It is important that the jugs with the greatest relative potential for failure and that may represent a risk to surface infrastructure be addressed first. Jugs located near the property boundaries of the mine site have the greatest risk to surface infrastructure (Figure 1c). Seismic-reflection surveys using compressional waves have been

demonstrated to be effective at delineating collapse structures at this site after a sinkhole has begun to form. However, at sites where the jug has not migrated completely through the Ninnescah Shale, compressional-wave reflection surveys would not provide sufficient information about material properties to confidently predict the location and intensity of tensional domes within the remaining shale overburden. Therefore, as part of this preliminary investigation into approaches appropriate for and capable of assigning priorities/relative failure risks to different jugs, shear-wave reflection and surface-wave imaging was used at four test wells selected for invasive sampling and borehole surveys, plus one well where relatively recent sonar data was available.

These five previously abandoned dissolution salt wells were selected as examples representative of the extremes in potential jug conditions and then drilled out to allow measurements to be made with a variety of borehole tools and techniques (Figure 16). Four well sites (#20, #39, #49, and #53) were known from historical plugging reports to likely have shale roofs and consequently salt jugs that could have migrated into the shale overburden. Dissolution mining in the other well (#86) had concluded and the well plugged, leaving a section of salt still separating the salt jug from the shale caprock as confirmed by the above-mentioned sonar survey. Measurement in the boreholes included a suite of electric logs and acoustic televiewer with sonar run inside each jug. All borehole and sonar data were consistent with the pre-drilling appraisal of the expected condition and location of the voids. At two of the locations (#20 and #53), the cavern roof was found to have migrated into the shale, while at the other two drilled locations (#39 and #49) the void roofs were still at or very near the top of the salt.

At each of these four sites, plus the previously sonared site (#86) a series of shear-wave surveys were conducted to evaluate the potential of measuring shear-wave velocities with sufficient accuracy to quantify any gradient over areas with elevated stress and therefore a relative increased potential for subsidence (Figure 16). Shear-wave reflection CMP surveying and MASW methods were evaluated. A total of eight shear-wave reflection profiles were acquired, two intersecting lines at each well location oriented as near orthogonal as possible. The orthogonal orientation was designed to investigate the potential for anisotropy (directionally dependent velocity), which could be indicative of preferential fracture orientation suggestive of a local structural trend. Originally the plan was to also acquire one MASW profile at each well location, but only two lines were completed following review of preliminary results.

Key to confident interpretation of reflections on CMP stacked section is the identification of coherent reflections on a reasonable number of representative shot gathers. This is particularly true for shear-wave data because the velocity of shear waves in the near surface is within 10% of surface waves. Compounding the problem the dispersive nature of surface waves can manifest itself on shot gathers in a fashion that appears to have curvature very similar to the NMO curves of reflections. To assist with the identification and optimization of shear-wave reflections on shot gathers, a downhole-velocity survey was conducted at well #39. From these downhole measurements, forward models were made that included reflections from the bedrock, "three finger dolomite," and upper Wellington Formation/Hutchinson Salt Member contact.

The program was ideally designed to measure the average velocity (NMO velocity) from the reflector to the ground surface with sufficient resolution and accuracy to detect changes in the shear velocity of at least 15% to 20%. This level of change was determined to be sufficient to exceed noise levels and rule out picking accuracy as the source of any observed changes in the shear-wave velocity across the spread. With the limited subsurface coverage allowed by these abbreviated spreads and restricted surface access (ideal would have been two lines intersecting at

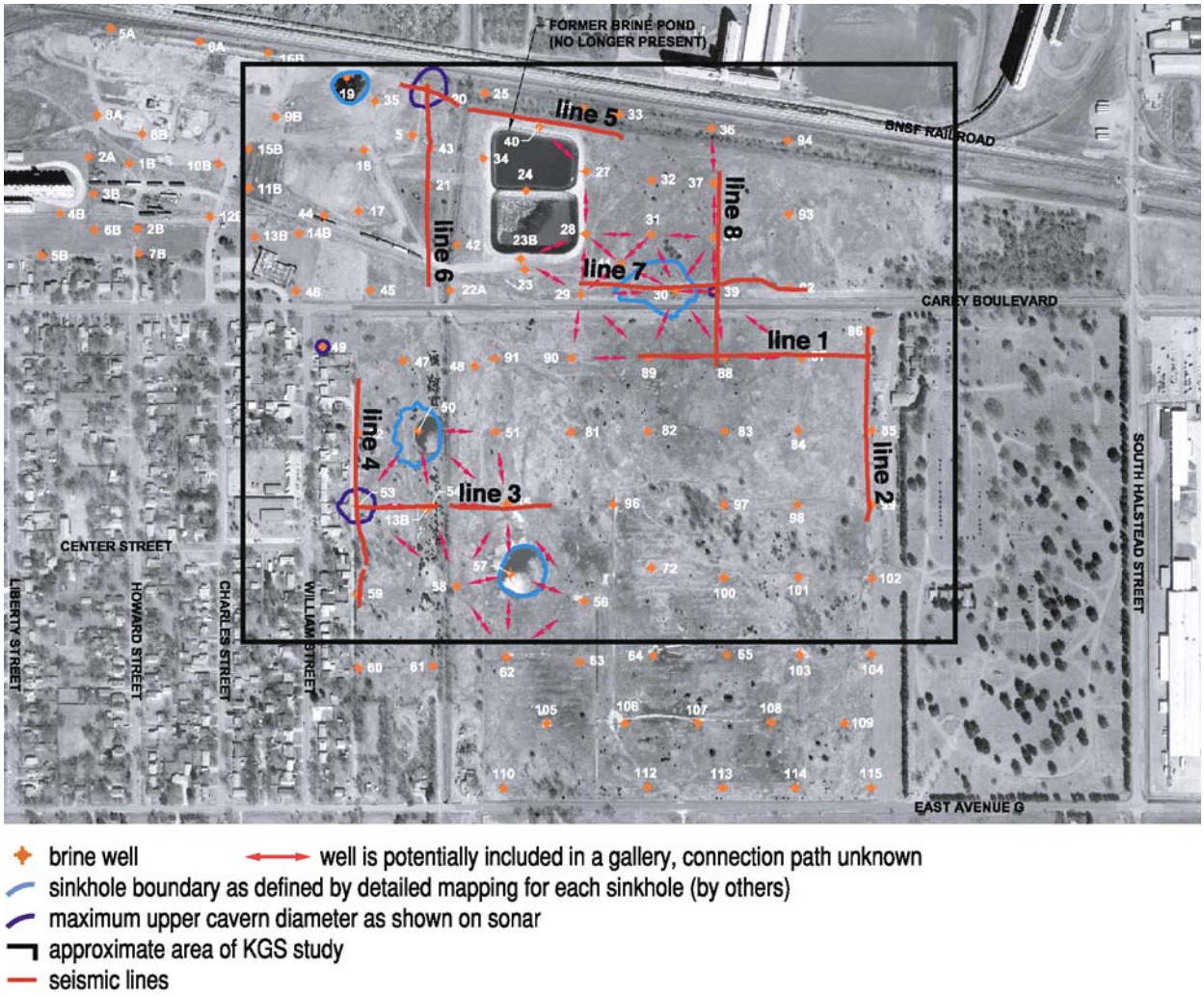


Figure 16. Aerial map of Mosaic legacy salt dissolution well field in Hutchinson, Kansas (from Burns & McDonnell), showing wells, galleries, sinkholes, sonar-determined jug diameters, and cultural features in the study area. Seismic lines from the KGS study are also indicated. Well offsets from seismic lines are presented in the Appendix.

half-way points on each fixed spread), optimal subsurface coverage at the target well location on both lines was not achieved. In most cases, because the principal wells of interest were located near the property boundaries, it was difficult to optimally locate the spreads for high fold imaging of the "three finger dolomite" much less the top of salt. Sufficient coverage and data were acquired to fully evaluate this shear-wave reflection approach for identifying zones with potentially elevated stress; however, none of the lines intersected and were equally split at the target well.

The question that this research ultimately needed to address was—does the enlarged, un-supported roof span characteristic of an upward-migrating void distort the stress field sufficiently to be detected as a change in shear-wave velocity on a CMP stacked section? We also hoped to investigate the possibility that stress build-up along the bedrock surface, postulated to be indicative of pre-failure, could be detected using inverted surface waves. All the experiments and analysis revolved around answering these questions and explaining the associated ancillary observations.

**Program Components and Results**

***DGPS rtk***

Each receiver station on the eight profile lines and any well head in proximity to the lines were located using Trimble 4700 and 4800 differential global-positioning system with real-time kinematic (DGPS rtk). The lines were laid out during acquisition following trails constructed using a dozer to scrape the upper 6 inches of loose soil and vegetation. This scraping process dramatically improved the coupling and reduced the near-source energy attenuation. This line preparation was very likely key, if not the reason for the extremely high quality CMP stacked sections. Actual station locations deviated from a straight line to avoid larger obstacles such as major drainage ditches, structures, fences, thicker and denser groves of trees, and wells (Figure 17).

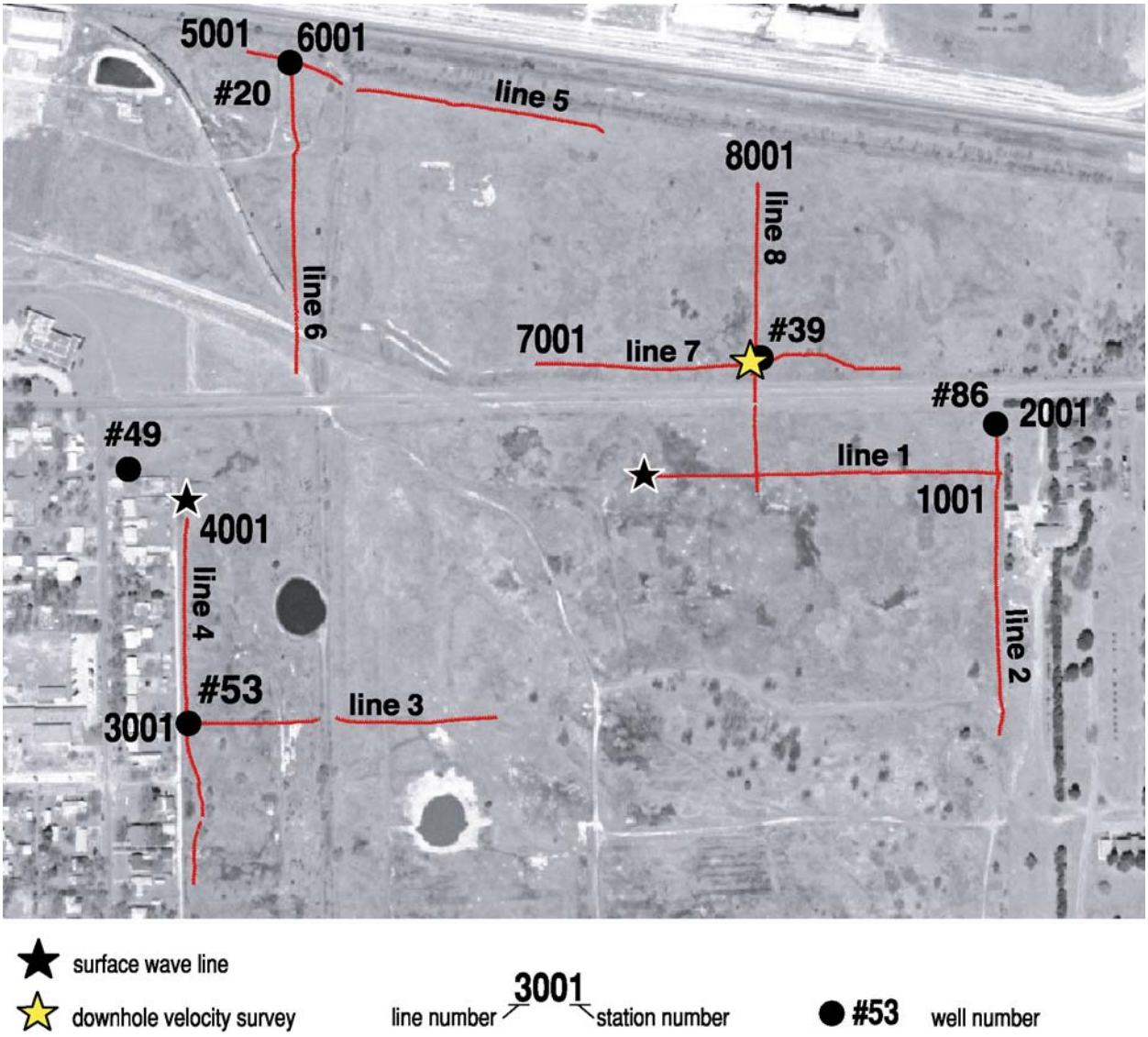


Figure 17. Orthophoto with only wells investigated by Burns & McDonnell, DGPS rtk measured seismic profiles, and line numbers. Numbered lines indicate reflection surveys and dark stars indicate lines with surface-wave profiles.

DGPS data were acquired using well #39 as the base and reference location for the site. Relative accuracy of each measured point is approximately 4 inches in each direction, X, Y, and Z. The beginning of each line started with station 1001 plus the line number. In a few locations DGPS data points were not acquired because of trees that were blocking the line of sight for satellites in the south sky.

Figure 18. GeoStuff hole lock and three-component geophone with controller.

***Downhole Velocity***

Surface-to-borehole data were acquired to get an accurate measure of the shear-wave velocity as a function of depth and to correlate the velocity function to key potential reflectors. Acquisition, processing, and interpretation of downhole data followed well-established guidelines (Hardage, 1983). As with most seismic methods, adapting methodologies developed in the oil industry to shallow targets requires deviating from accepted "rules of thumb." Near-vertical offset VSP (ZVSP) style of acquisition provides the best measure of velocity as a function of depth and was therefore the method used for this study. With no compass and therefore no potential for orienting the downhole receiver, relative amplitude response from the two orthogonal, horizontal, co-located downhole receivers was used to guide the interpretation of the first arrival for each depth and then to calculate the shear velocity (Figures 18 and 19). Two source orientations were used at each depth to ensure at least one of the four recorded traces possessed shear-wave signal within 45 degrees of proper polarization.

Figure 19. 3-C hole lock geophone with band deployed.

Downhole data were acquired in well #39 and included 15-recorded shots per receiver-depth interval. With the top of the Hutchinson Salt Member approximately 400 ft below ground surface, the downhole geophone was lowered to 380 ft, locked in place, data were recorded, and then unlocked and moved up the borehole 20 ft. This sequence was repeated until the receiver reached the top of the well. One 40-Hz surface geophone was placed near the well to ensure the time zero was accurately recorded (start time is critical for this kind of survey) (Figure 20). A sledgehammer impacting a metal striker plate was used to generate compressional wave energy, and that same sledgehammer impacting the ends of a block (square post, 3 ft long with steel end caps and cleats) produced the horionally polarized shear

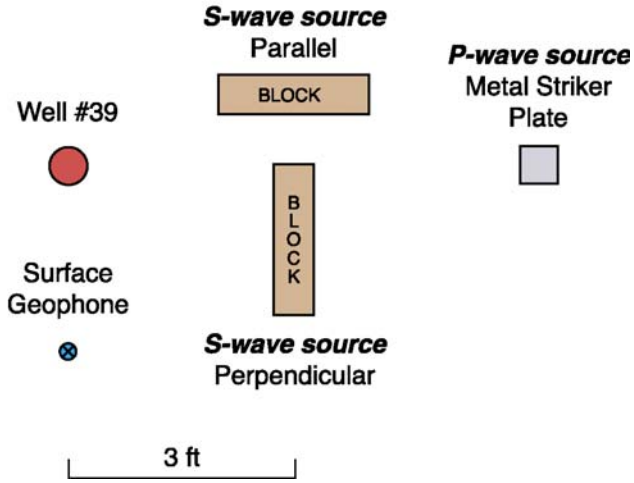


Figure 20. Configuration of downhole seismic-velocity measurements at well #39.

energy. At each receiver station data were recorded from five vertical impacts, five north to south horizontal impacts, and five east to west horizontal impacts, resulting in 15 total shots recorded per station. The source impact points were 3 ft from the wellhead.

Shear-wave downhole-depth gathers possess sufficient signal-to-noise ratio to make confident first-arrival picks (Figure 21). From these first-arrival picks a velocity (feet downhole divided by energy-arrival time) function relative to depth was generated (Figure 22). Forward models were generated using this velocity function and depth to key interfaces from drill data to allow simulation of two-way travel time and reflection geometry on a shot gather. This synthetic model was used to both optimize the acquisition parameters and interpret the shot gathers. Downhole data of this type are a critical component of any seismic-reflection survey where depth is measured in time.

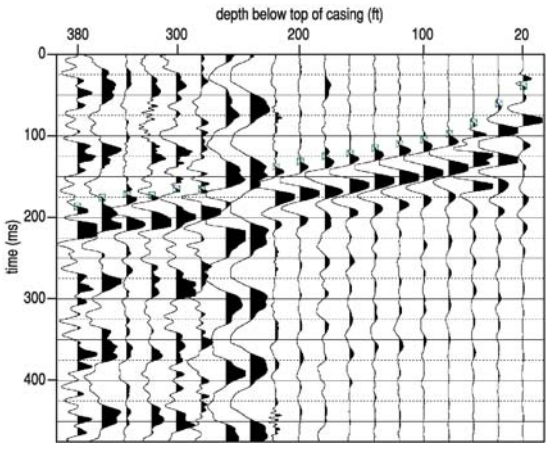


Figure 21. Downhole shear-wave survey acquired in borehole #39. Dramatic change in noise levels is due to rotation of the borehole geophone, which was accounted for using records acquired with various source-receiver geometries.

### *Reflection*

A properly designed and executed high-resolution S-wave seismic-reflection survey should be capable of mapping key reflectors above the shale/salt interface at this site. Shear-wave velocity changes associated with stress build-up over these salt jugs will be distributed through a reasonably substantial portion of the shale overburden. To measure changes in the shear-wave velocity reflector, NMO velocities are estimated to establish an average velocity between the reflector and ground surface. With reflections from bedrock, the "three finger" dolomite, and top of salt, the overburden can be well differentiated.

Shear-wave reflection data from this site were acquired using a fixed-spread deployment where the source was 'walked' through the spread producing a uniformly increasing fold from each end of the spread toward the middle. With a total spread length of around 780 ft and walk-through approach to acquisition, a cone-shaped imaging geometry resulted with reflecting points from the top of the salt only imaged near the center of the spread. This acquisition style was necessary due to limited surface access and a focused subsurface

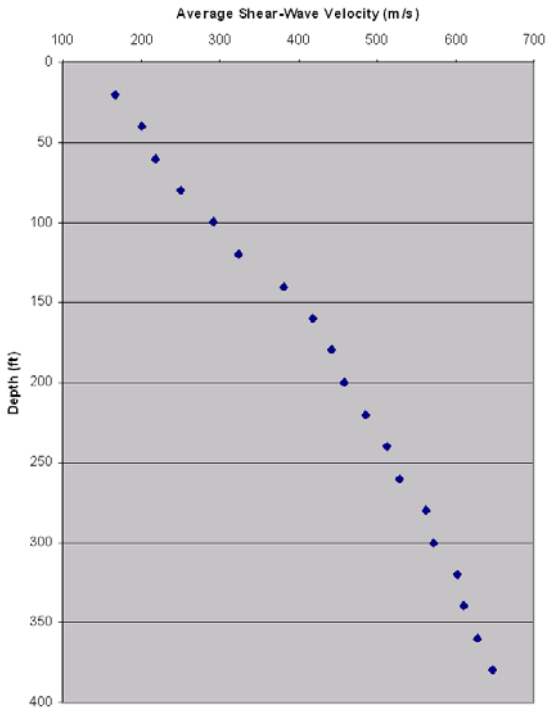


Figure 22. Graph displays changes in average velocity with depth for the downhole-seismic survey conducted at well #39. Interpreted velocities were used to create the synthetic gather displayed in Figure 23. Trace polarity was reversed on several traces to account for changes in component orientation and rotation of the downhole geophone prior to picking.

target. The cone-shaping imaging geometry is a drawback of this method, effectively reducing the lateral subsurface image as a function of depth. Proven high-resolution techniques were used to design the data-acquisition parameters and to determine optimum equipment and methodologies (Steeples and Miller, 1990).

With the placement of the lines constrained by obstacles on-site as well off-property structures and restrictions, recording data with optimal redundancy and subsurface coverage was not possible. With the variability in subsurface coverage relative to the particular jugs of interest, in many cases only a single line sampled the key subsurface interval of these target jugs. The seismic source, geophone type, spread geometry, shots/point, and acquisition philosophy were based on the survey objectives, site limitations, and models based on the downhole velocity analysis. An elastic model was used to generate a synthetic shot gather, with reflections returning from the bedrock surface, "three finger" dolomite, and salt correlating remarkably well with a shot gather from line 1 (Figure 23). Acquisition, processing, and interpretation proceeded with high confidence based on the excellent match between the model and real data.

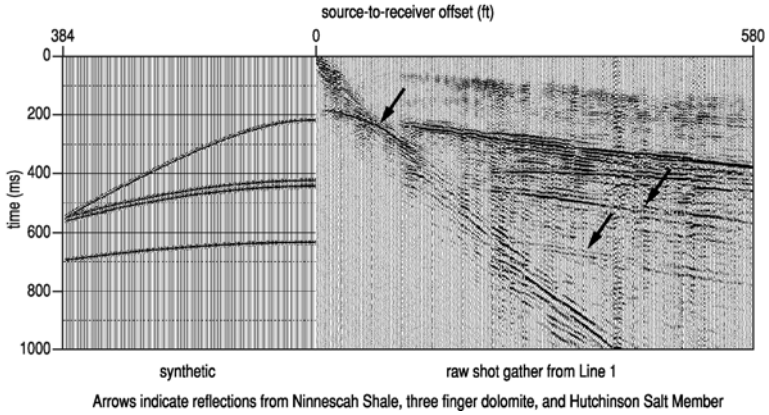


Figure 23. Comparison between synthetic and real shot gather. Synthetic, generated with velocities calculated from the uphole survey in well #39 and reflectors identified from borehole logs, is compared to a raw common-source gather from line 1. Reflections from the top of the upper shale, dolomite, and salt, indicated by arrows, are in reasonable agreement with those from the synthetic gather.

***Data Acquisition***

Eight maximum 120-fold, common-midpoint (CMP) shear-wave reflection lines were acquired at four different locations, with two perpendicular lines intersecting as near the target well as possible (Figure 17). Each fixed spread consisted of 240 14-Hz horizontal geophones each separated by 3.25 ft, resulting in a total spread length around 775 ft (Figure 24). The source was an IVI Mini-Vibe I with its mass configured to produce the $S_H$ component of the shear-wave energy field and waffle-style base plate (Figure 25). Three 10-second-long 15-Hz to150-Hz upsweeps were recorded at each source station. Source stations were separated by 6.5 ft, with the first source station at the first receiver station and the last source station near the 240th receiver station. Data were recorded on four, 60-channel Geometrics StrataView seismographs networked into a StrataVisor controller (Figure 26). The resulting 24-bit uncorrelated data included 12,000 samples per trace uniformly acquired over the 12-second record length. To optimize the source and receiver coupling and reduce statics, a bulldozer was used to clear each line of vegetation and the upper few inches of soil (Figure 27).

Figure 24. IVI Minivib crossing Carey Boulevard near the end of line 8.

Figure 25. 14-Hz Geospace shear-wave geophones with level bubble to optimize SH response.

Figure 26. Geometrics 240-channel seismograph during acquisition of reflection data on line 8.

Figure 27. Seismic recording vehicle located near the north end of line 6.

***Processing***

Data were processed using an approach designed to optimally enhance near-surface reflections. Shear-wave-reflection data present a slightly different set of problems than compressional-wave data, which represents the vast majority of all seismic-reflection data. The polarized nature of shear-wave energy provides somewhat of a natural filter to most high-amplitude cultural noise, which travels as compressional waves. However, with the velocity of shear-wave energy approximately 1.1 times that of surface waves, shallow reflections from unconsolidated sediments and bedrock are many times very difficult to separate from dispersive surface-wave energy. At this site the bedrock reflection was well formed and therefore easily separated from surface-wave energy. Deeper reflections were pronounced and recorded within the optimal window. The processing flow was a customized version of processing flows routinely used for near-surface and/or high-resolution compressional-wave data (Figure 28).

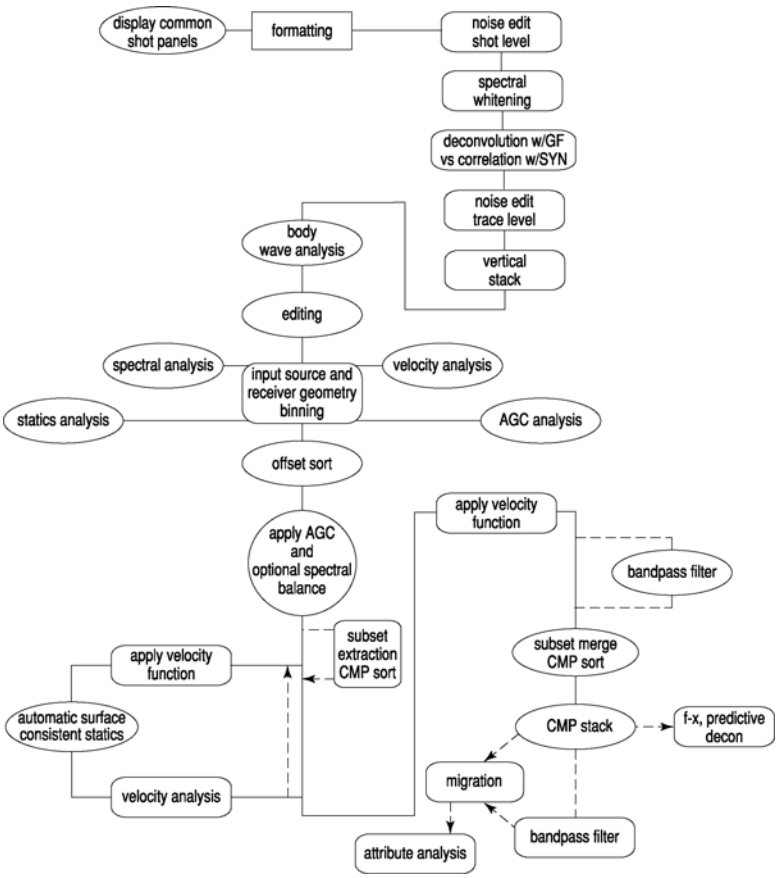


Figure 28. Generalized shear-wave reflection processing flow.

***Results***

CMP stacked reflection sections provide a view of the subsurface limited by the resolution and signal-to-noise ratio of the data. Reflections on stacked sections possess several characteristics that are indicative of the properties of the earth between the ground surface and the reflector as well as the reflector itself. Changes in the amplitude, frequency, or phase of the earth response wavelet or pulse can be diagnostic of the material or changes in material across an interface. For this study the amplitude, signal-to-noise ratio, and arrival time of the stacked reflection is important, but most importantly is the calculated NMO velocity of the reflected shear-wave pulse between the reflector and ground surface. Systematic changes in that velocity from the 'norm' that can be correlated to the current condition of the roof rock of abandoned jugs at this site could be a key for predicting vertical void migration characteristics and the collapse mechanism.

Four well sites (#20, #39, #49, and #53) were selected for invasive investigations and characterization of their current condition (Figure 17). These wells were selected based on the characteristics of the jug and overburden at the time each was plugged. One well was associated with a void that, based on an available recent sonar survey, at the time it was plugged still possessed a salt roof with the majority of the void volume in the deeper portion of the salt interval (well #86) (Figure 17). Two wells had jugs that were known to have migrated into the shale overburden at the time they were plugged (well #20 and well #53) (Figure 17). The four wells that were drilled out had a suite of geophysical logs and an acoustic televiewer run in the borehole with sonar data acquired in the open portion of the jug (Figure 29). The condition of

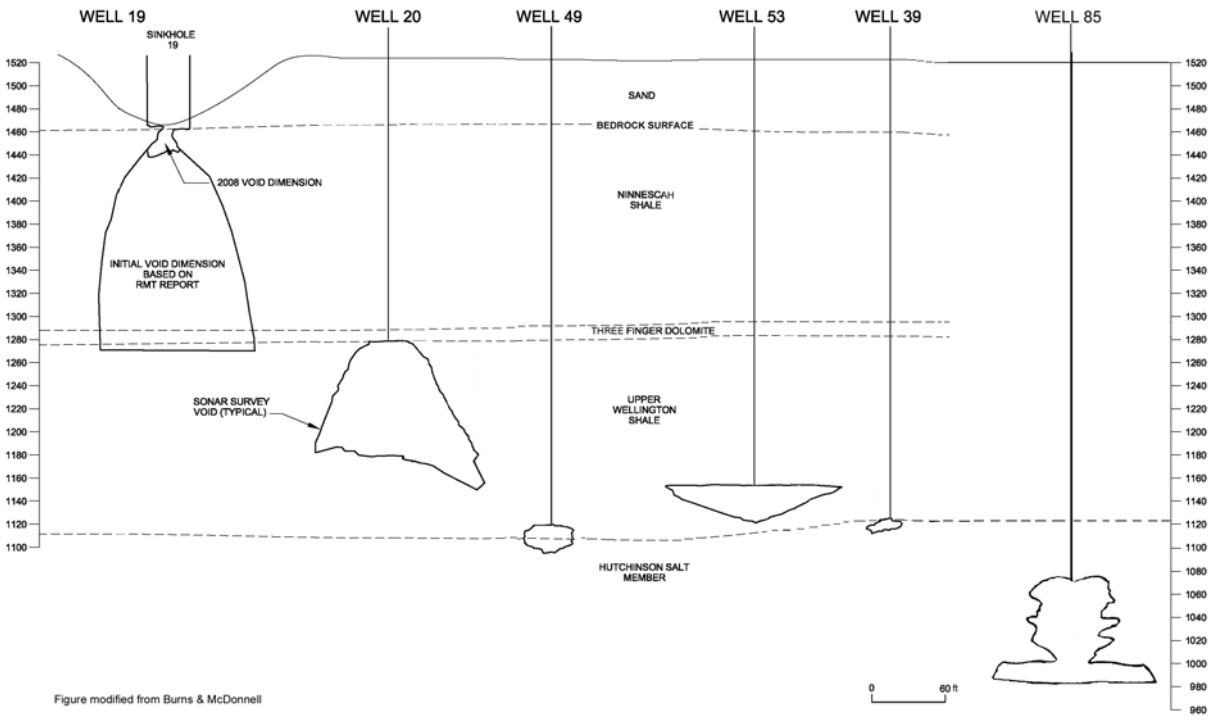


Figure 29. Drill-confirmed void location and geometry modified from a figure provided by Burns & McDonnell.

the jugs themselves, the roof of the jugs, and the shale/salt contact were ascertained as well as an appraisal of the current condition and estimate of the relative collapse potential for each jug.

Seismic reflection line 1 was acquired from west to east starting south of well #86 and line 2 was acquired north to south starting north of well #86 (Figure 17). The CMP stacked section of line 1 possesses excellent quality reflections from the bedrock, top of the "three finger" dolomite, and the top of the salt (Figure 30). Reflections have sufficient coherency to confidently pick NMO velocities within 10% from CMP gathers. Since the salt jug beneath well #86 was classified as either a salt cavern with a thick salt roof or a small jug near the salt/shale contact, these data and measured properties provide a representative sample or baseline. The salt reflection is clearly evident but possesses a lower amplitude relative to the other reflections because of its relative depth in the section and the reduced fold that is also a function of depth. The portion of the salt/shale contact imaged on this section is several hundred feet south of well #86. As previously described, this skew in subsurface sampling is related to the spread geometry, acquisition method, and access restrictions. Fortunately, this profile does image well #85, which was contemporaneous with #86 (i.e., post-1975 era, when State regulations required that a salt roof be left in place) and has a similar salt roof based on recent sonars. Jugs in this part of the state are considered to be in good condition with the top of void separated from the salt/shale contact by a reasonable thickness of salt. The sonars of these two caverns are so similar they can be considered analogous.

Line 2 was acquired from north to south with well #86 100 feet or so south of the beginning of the line (Figure 17). The CMP stacked section of line 2 has a good quality reflection from both the bedrock and the "three finger" dolomite, but has only a hint of the salt/shale contact (Figure 31). Unique to the dolomite reflection on this profile is the apparent structure near the center of the line at station 2110. This structure could be real or it could be a velocity

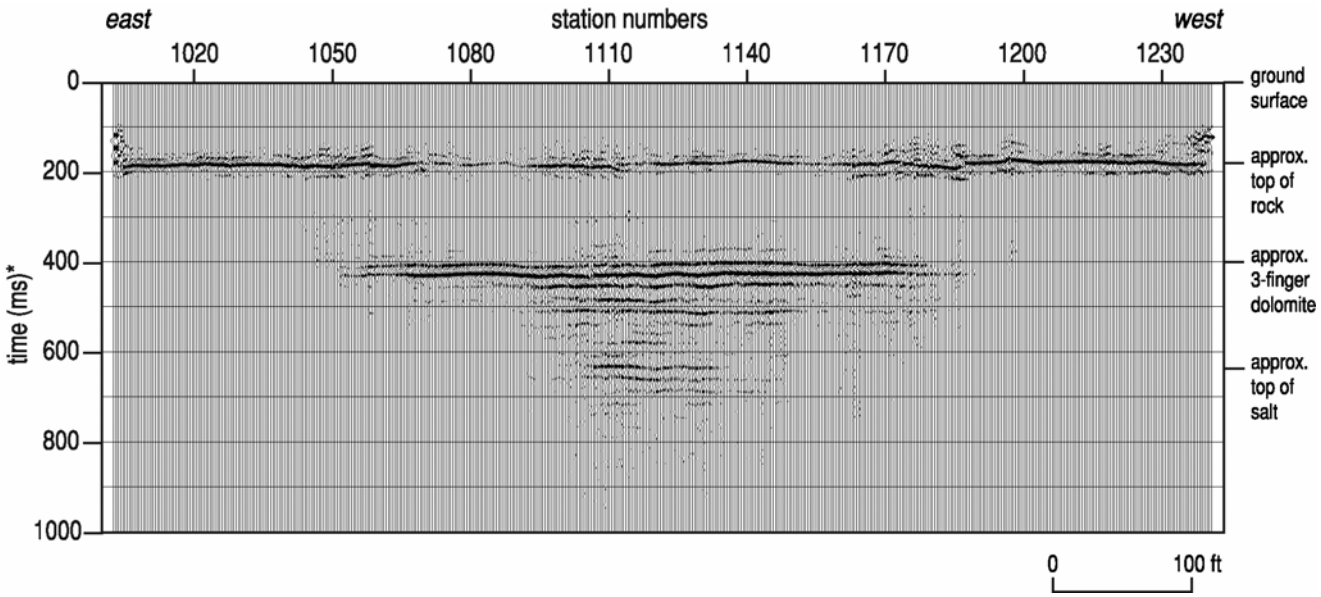


Figure 30. E-W oriented CMP stacked section from line 1, acquired south of Carey Boulevard and adjacent to the cemetery. The bedrock reflection is at ~180 ms and the top-of-dolomite reflection is at ~400 ms. A hint of the top of salt can be seen at ~620 ms. Data were acquired using a fixed receiver spread with the source rolled through from one end to the other, resulting in a smaller "imaging window" with depth, i.e., longer lines would be necessary to image the deeper reflections at greater extents.

*See Figure 4 for approximate depth correlations.

pull-up indicative of a higher velocity zone in the sediments above this reflection relative to the velocity on either end of the imaged dolomite. In any case, this apparent structure is not a direct measure of the salt caverns. The high signal-to-noise ratio is quite promising as it relates to the potential use of this approach for locating jugs under elevated stress.

Line 3 intercepts line 4 to form a 'T' with target well #53 located at the far west end of line 3 (Figure 17). The line 3 crosses over well #54 at approximately station 3086 and well #55 at approximately station 3171. An approximately 10-ft-deep drainage ditch located near the center of this profile represented a significant static anomaly and drop in vibrator coverage. A drop in coherency and decreased signal to noise in the bedrock reflection is likely due to this drop in source continuity, but reflections from the dolomite and salt will not be noticeably affected (Figure 32). The dolomite reflection is very interpretable at around 450 ms, but the salt reflection, expected to be evident at around 650 ms, is not obvious. An apparent localized increase in NMO velocity can be interpreted near well #54.

Most noteworthy on this line 3 section are the apparent diffractions and broken nature of the dolomite near station 3120. Considering the horizontal resolution of these data, this feature is consistent with a collapse structure that has breached the dolomite interval. If this is a failure in the dolomite layer, then it is very possible the salt/shale contact has been significantly disturbed in this area and would not result in a coherent reflection. Station 3120 is between wells #54 and #55, which were known to have been operated in gallery, with the position/depth of the gallery connection not known. Since the disturbed section of the dolomite is not directly over an existing cavern, it could have been caused by a collapse of the gallery connection, or comprise a natural dissolution feature. If it was caused by a collapse of a gallery connection, it has apparently not extended upward to impact the ground surface.

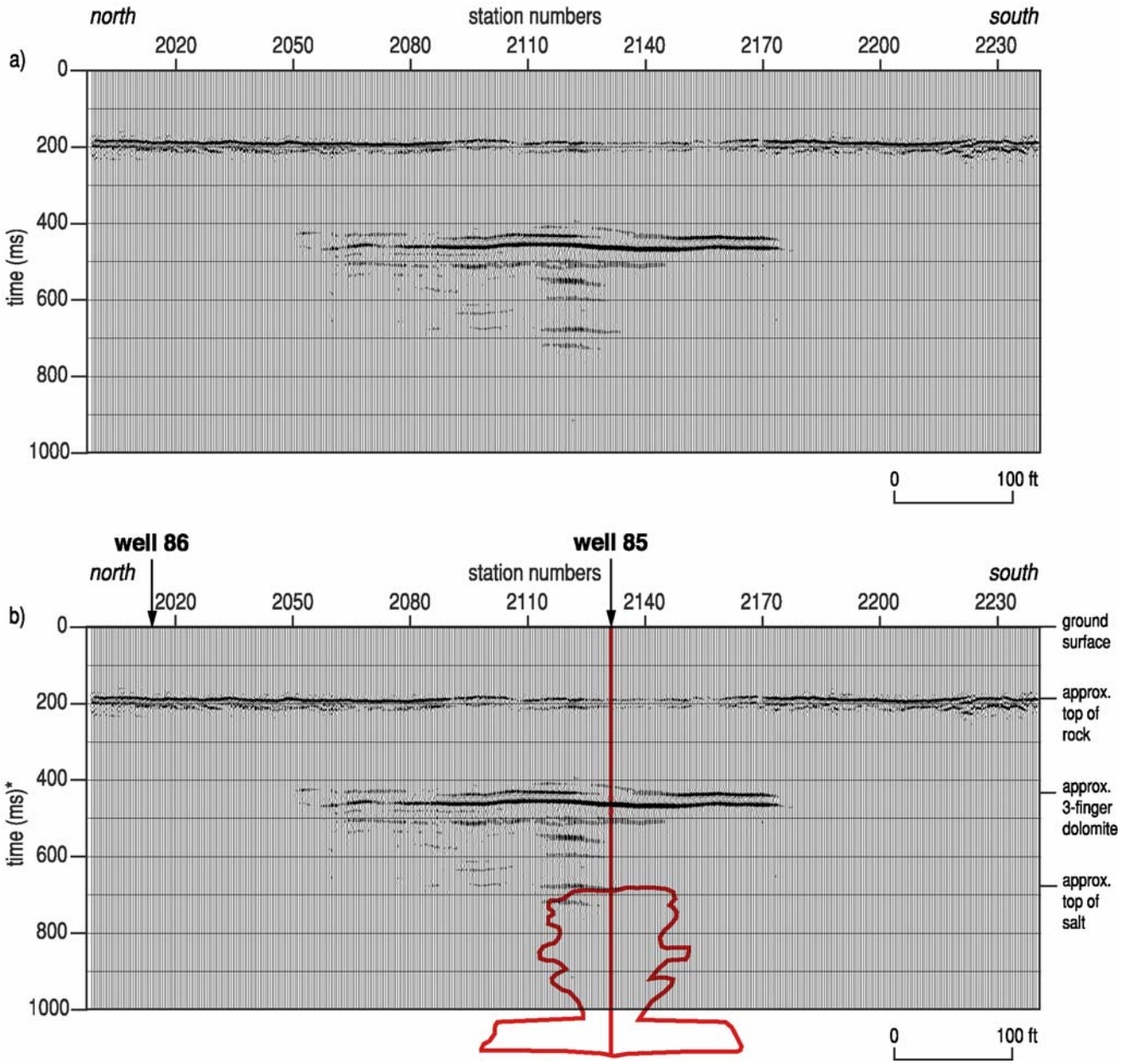


Figure 31. (a) N-S oriented CMP stacked section from line 2, acquired at the same location as, but perpendicular to line 1. Bedrock and dolomite reflections are located at ~180 and 420 ms, respectively. Stacking velocities are relatively consistent across the line. (b) Approximate location and cross section of sonar-interrogated jug superimposed on seismic section beneath well #85. The relative positions of the wells and cavern sonar surveys superimposed on the seismic section were based on relative approximate locations, shapes, and depths, not interpreted from seismic results. Superimposition was performed by Burns & McDonnell. Dashed geometry and size of jug beneath well is approximately based on tonnage removed and historical borehole data while solid lines are derived from modern sonar, modern geophysical logs, tonnage, and historical borehole data. Well #85 is located 16 ft east of station 2131 and well #86 is located 16 ft east of station 2007.

*See Figure 4 for approximate depth correlations.

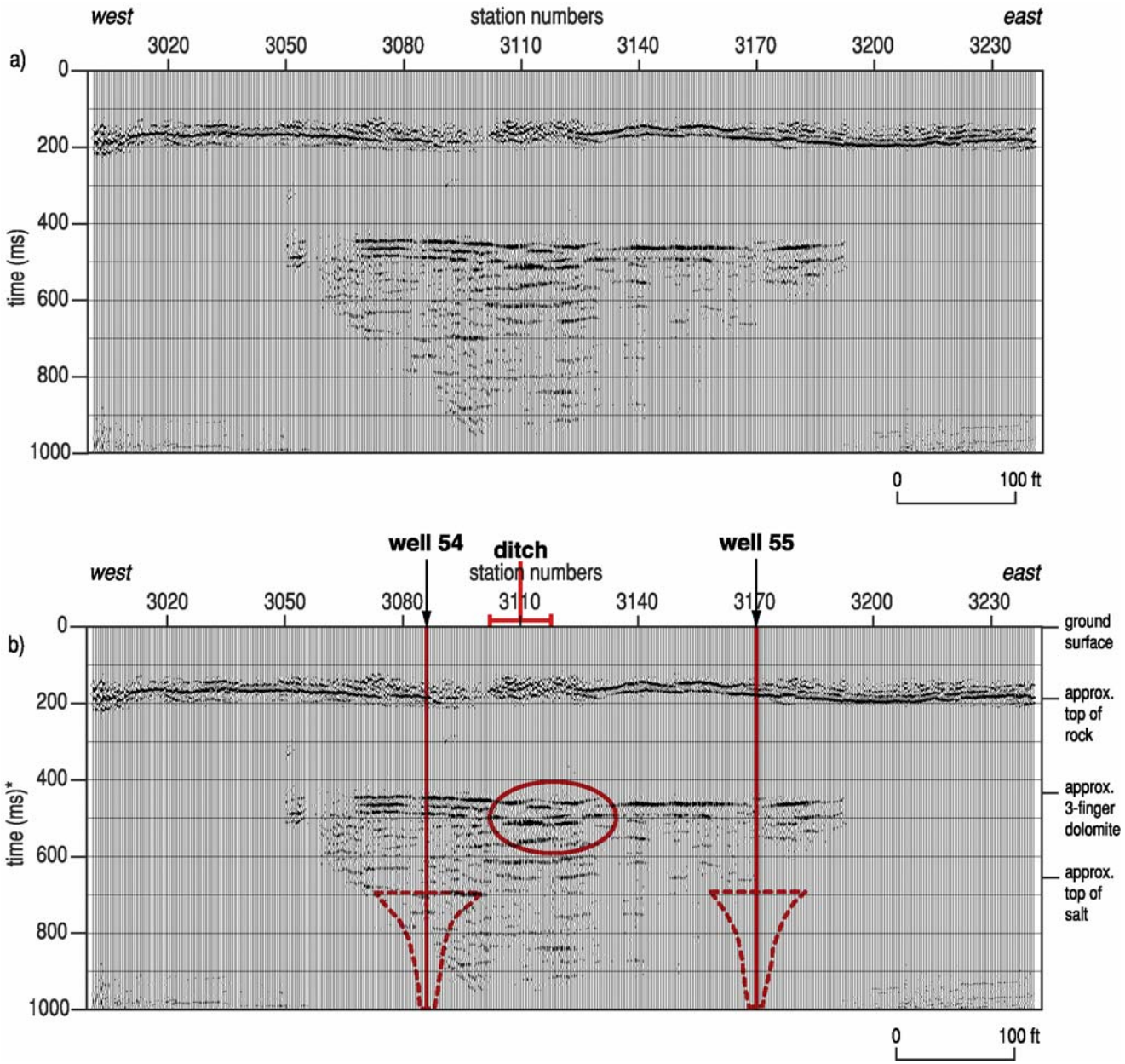


Figure 32. (a) W-E oriented CMP stacked section from line 3, which originates near the west property boundary and intersects line 4 near well 53. (b) Approximate location and cross section of jugs beneath wellheads #54 and #55 superimposed on seismic section based on historical data and current condition of nearby wells. The relative positions of the wells and cavern sonar surveys superimposed on the seismic section were based on relative approximate locations, shapes, and depths, not interpreted from seismic results. Superimposition was performed by Burns & McDonnell. Dashed geometry and size of jug beneath well is approximately based on tonnage removed and historical borehole data while solid lines are derived from modern sonar, modern geophysical logs, tonnage, and historical borehole data. The circle indicates a disturbed area near station 3120. Well #54 is located on the line at station 3091 and well #55 is on the line at approximately station 3170.

*See Figure 4 for approximate depth correlations.

Line 4 is the north to south line that straddles well #53 (Figure 17) and begins nearly adjacent to well #49. Reflections from this profile are of good quality with some drop in signal-to-noise ratio relative to lines 1 or 2 (Figure 33). There could be several reasons for this drop in overall data quality, but the key thing to note is the stacking velocities can still be estimated with a picking error of less than 10%. Well #52 is located at station 4070 and is consistent with an obvious drop in bedrock and dolomite reflection coherency, and in this case it also corresponds to a marked drop in stacking velocity. Using the theory that governs shear-wave velocity, this could relate to a drop in the shear modulus, which would be consistent with a zone of reduced stress. Reduced stress would be indicative of a collapse structure. Dolomite reflections coincident with well #53 (CMP 4161), which is known to be consistent with a void that has migrated several tens of feet into the shale overburden, exhibit elevated stacking velocities relative to dolomite reflections in areas without voids. This increase could be related to elevated stress.

The CMP stacked section along line 5 runs sub-parallel to railroad tracks along the northern boundary of the site (Figure 17). Due to site limitations the profile runs parallel to the northernmost line of wells and only the very beginning of the line, near the west end, ties to well #20. Reflections from the bedrock and dolomite are obvious (Figure 34). Drops in amplitude of the bedrock reflection have not interfered with the confidence in estimating NMO velocities. Some of this drop in amplitude is related to a drop in fold that occurred as a result of the large drainage ditch between stations 5079 and 5093. Site access problems allowed only bedrock reflection coverage beneath well #20; however, a portion of well #25—which is of similar age—was imaged and an elevated velocity was observed. This, of course, could be indicative of an elevated stress field. The wellhead for cavern #25 is offset to the north of the seismic line by about 60 feet. Well #40 is offset from the seismic line about 30 feet at about Station 5171 and has been estimated using solution mining records to have been of substantial size. The dolomite reflection beneath station 5171 clearly possesses a different character and elevated arrival time. The apparent offset at around station 5155 could be related to the condition of cavern #25.

Line 6 is a north-to-south line that intersects line 5 at station 5020 and well #20 (Figure 17). This line was constrained on the north by the railroad property line and therefore did not sample any subsurface potentially affected by well #20. Reflections from bedrock are at around 200 ms and possess reasonable coherency across the line with only minor undulations in their otherwise flat appearance (Figure 35). A strong reflection from the dolomite sequence arrives at around 450 ms with a good signal-to-noise ratio. Two relatively small caverns (based on solution mining records and some reasonable assumptions) occur beneath about stations 6073 (well #43) and 6114 (well #21). An interesting anomaly in the otherwise flat dolomite reflection can be interpreted at around station 6125. This somewhat vertical feature is also present on the salt reflection arriving around 200 ms later. Focusing on the geometry of this feature there appears to be a ‘plug’ missing from the dolomite reflector with a shallower reflection spanning that gap in the dolomite reflection. This anomaly can be traced to the salt reflection where it manifests itself as a gentle fold-like feature. Station 6125 is near well #21. Since none of the wells in this area were reported to be operating as a gallery, the presence of this anomaly is a mystery.

CMP line 7 is an east-to-west profile that intersects well #39 and well #30 (Figure 17). Well #39 was recently investigated with sonar and determined to have a small void (approximately 35 feet in diameter) located at the salt/shale interface (Figure 29). Well #30 is approximately centered on a shallow sinkhole that formed in the 1990s and previously investigated with

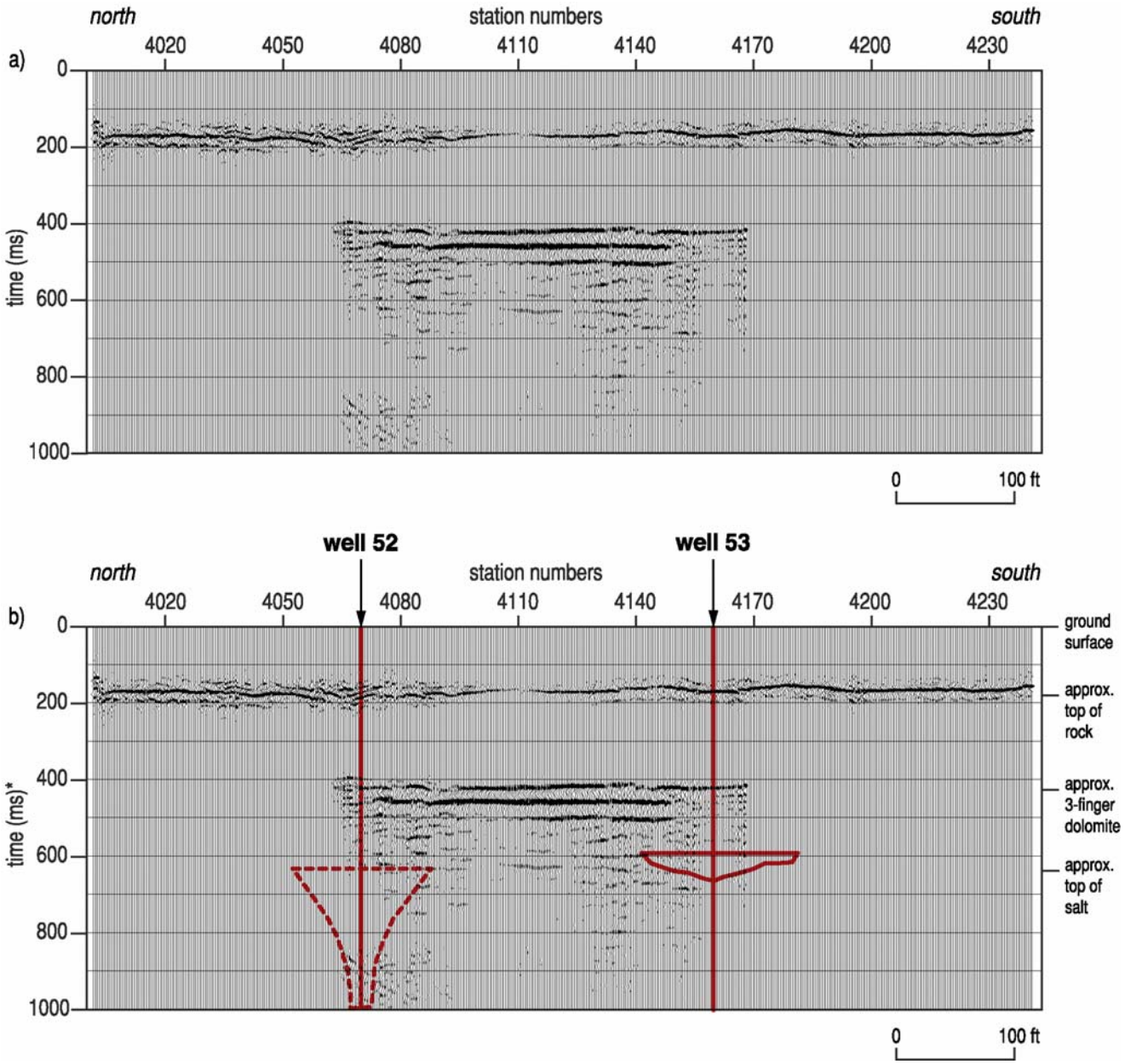


Figure 33. (a) N-S oriented CMP stacked section from line 4, acquired south of Carey Boulevard and adjacent to the neighborhood on the west side of the property. The bedrock and dolomite reflections are located at ~170 and 420 ms, respectively. Well #52 is located at station 4070, which corresponds to a disruption in the bedrock and dolomite reflections. Stacking velocity of the dolomite reflection is lower at this location relative to the rest of the line, suggesting failure of the roof rock and fracturing of the upper shale. Well #53 coincides with station 4161. Stacking velocities exhibit an increase relative to the rest of the line, which may indicate higher relative stress of the roof rock at this well. (b) The approximate cross section of the jugs and depth is superimposed on seismic section based on current sonar data for well #53 and historical data for well #52. The relative positions of the wells and cavern sonar surveys superimposed on the seismic section were based on relative approximate locations, shapes, and depths, not interpreted from seismic results. Superimposition was performed by Burns & McDonnell. Dashed geometry and size of jug beneath well is approximately based on tonnage removed and historical borehole data while solid lines are derived from modern sonar, modern geophysical logs, tonnage, and historical borehole data. Well #52 is located on the line at station 4070 and well #53 is located on the line at station 4161.

*See Figure 4 for approximate depth correlations.

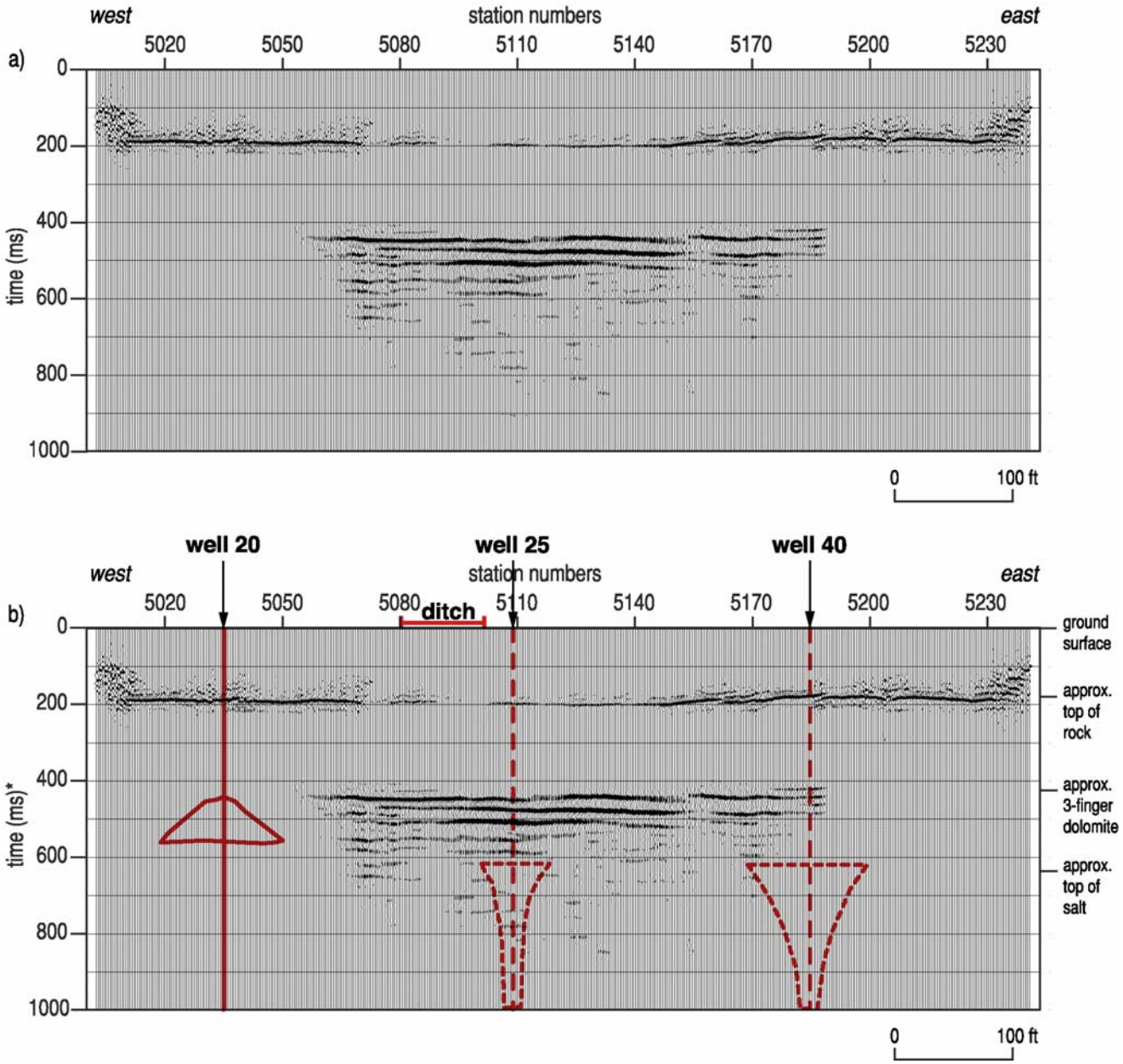


Figure 34. (a) W-E oriented CMP stacked section from line 5, acquired north of Carey Boulevard and adjacent to the railroad tracks to the north. The bedrock and dolomite reflections are located at ~180 and 430 ms, respectively. A ditch coincided with stations 5079-5093, creating a gap in the data and lower fold relative to the rest of the line. Well #25 is approximately located at station 5140, which coincides with relatively higher stacking velocities of the dolomite reflection. (b) Approximate cross section for salt jugs recently measured with sonar in well #20 and estimated from historical data for wells #25 and #40. The relative positions of the wells and cavern sonar surveys superimposed on the seismic section were based on relative approximate locations, shapes, and depths, not interpreted from seismic results. Superimposition was performed by Burns & McDonnell. Dashed geometry and size of jug beneath well is approximately based on tonnage removed and historical borehole data while solid lines are derived from modern sonar, modern geophysical logs, tonnage, and historical borehole data. Well 20 is located 7 ft north of the line at station 5035, well #25 is located approximately 75 ft north of the line near station 5110, and well #40 is located about 16 ft south of the line at station 5183.

*See Figure 4 for approximate depth correlations.

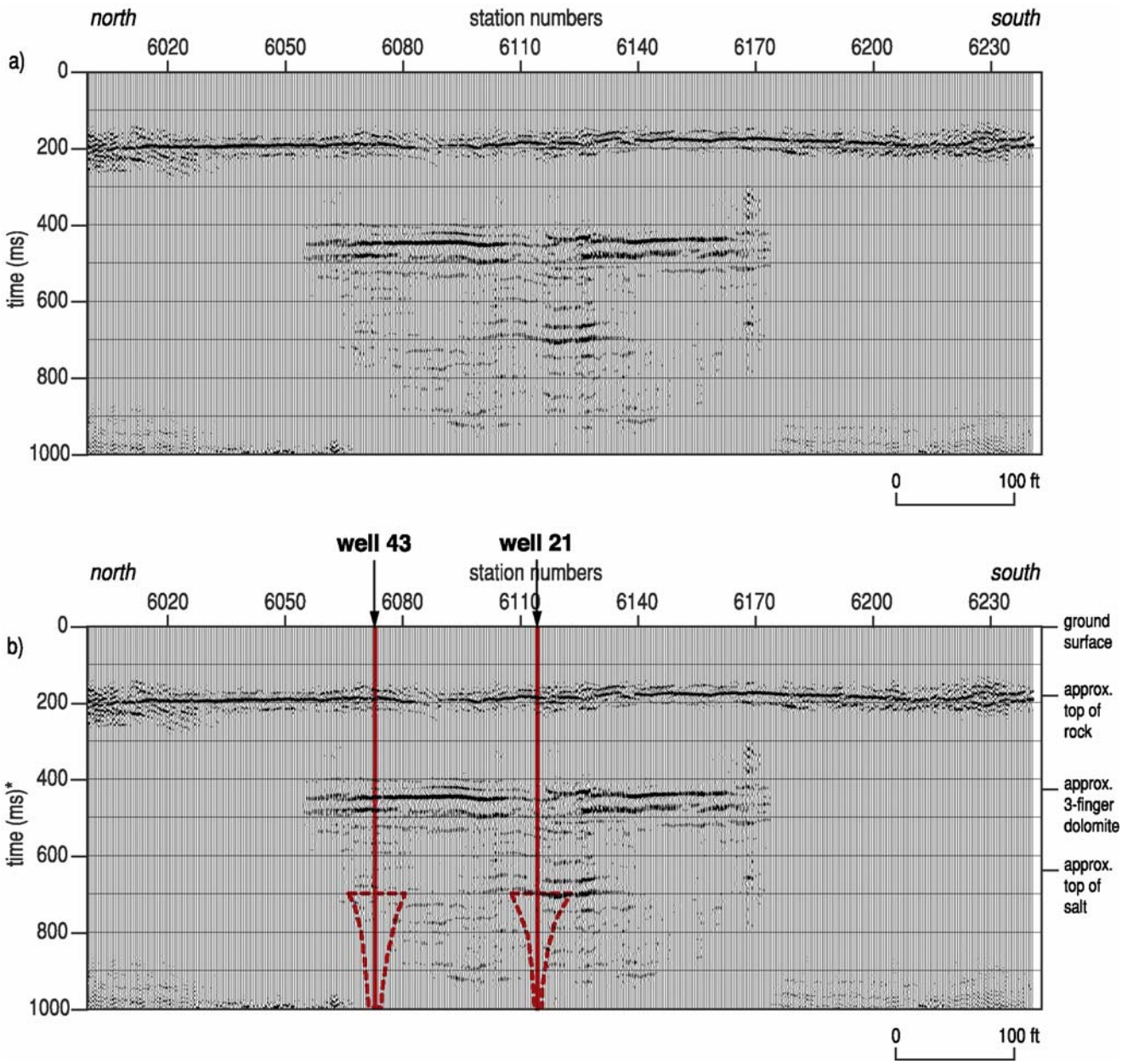


Figure 35. (a) Line 6 intersects line 5 near the north property boundary at well #20. Due to the subsurface coverage of lines 5 and 6, they do not overlap in the subsurface and therefore there is no hard tie point. (b) Approximate cross section of salt jugs superimposed on seismic sections with wells #21 and #43 based on historical data. The relative positions of the wells and cavern sonar surveys superimposed on the seismic section were based on relative approximate locations, shapes, and depths, not interpreted from seismic results. Superimposition was performed by Burns & McDonnell. Dashed geometry and size of jug beneath well is approximately based on tonnage removed and historical borehole data while solid lines are derived from modern sonar, modern geophysical logs, tonnage, and historical borehole data. Well #43 is located on the line at station 6069 and well #21 is located on the line at station 6117.

*See Figure 4 for approximate depth correlations.

compressional-wave seismic reflection. Well #30 is located at approximately station 7902 and well #39 is located near station 7144 (Figure 36). With surface failure observed at well #30, the shear-wave velocity in this area should be lower than what is considered normal. In fact the drop in signal-to-noise ratio and a decreased stacking velocity are both prime criteria for evaluating the stress regime of voids. This observation represents more physical evidence corroborating the theoretical based suggestion that seismic velocity measurements can be used as predictors of vertical void migration.

Line 8 is the north to south line that crosses well #39 and line 7 (Figure 17). This line crosses cavern #38 at about Station 8063. Reflections from line 8 all possess good coherency and are consistent with a relatively undisturbed subsurface (Figure 37). A slightly chaotic bedrock reflection is obvious between stations 8140 and 8200 and is likely related to the gravel road, drainage ditch, paved road, and railroad tracks crossed between those stations. The far south end of this line was heavily undermined by prairie dogs, but as evident by the coherent and well-behaved bedrock reflections, the disturbed shallow soils have no effect on reflection signal. The dolomite reflection at 450 ms is coherent and uniform with no indications of deformation related to subsidence. There is only a slight hint of a salt reflection near a time depth of 650 ms. Without a doubt, the surface alterations between 8140 and 8200 had some influence on signal propagation. It is not completely clear what characteristics control where around this site energy propagation is sufficient to produce salt reflections; it is likely a complex combination of several factors including soil coupling, collapse features, surface alterations/fill/old buried structures, and surface obstacles.

With the elastic moduli being dependent, at least in part, on the stress/strain relationship and the relationship of the shear-wave velocity to the shear modulus, predictable variations in NMO shear-wave velocity relative to the condition of known voids provide strong empirical evidence supporting the hypothesis that shear-wave CMP reflection data can be used to classify the relative strength of the stress field above voids. Some relative measure of roof-failure risk can be developed based on measured shear-wave NMO velocity. This relative estimation of risk considers the approximate strength of various roof rocks within the overburden and the stage of migration each is at en route to the ground surface related to the shear-wave NMO velocity at each jug location. From the eight lines acquired and processed at this site, combined with the results of the invasive analysis, several striking observations can be made that provide both empirical and theoretical basis for ranking the potential for vertical movement of an individual void.

Comparison of the stacking velocities from the bedrock and dolomite reflectors along each of the profiles compared to the locations of the dissolution well bores allows specific observations to be made concerning relative shear-wave velocities (Figure 38). Fortunately for comparison reasons, the bedrock reflections across the site possess a relatively consistent stacking velocity. This generally consistent average velocity in the unconsolidated sediments all but eliminates the possibility that the observed relative changes in shear-wave velocities between the dolomite and ground surface are related to changes in the alluvium. Therefore, any relative differences in velocity can be attributed to changes in the properties of the shale unit between the dolomite and bedrock surface.

For comparison purposes, line 1 should be indicative of an area with virtually no build-up in stress related to voids in the salt, while line 5 on the other hand is over voids that are known to have migrated a significant distance into the shale and therefore likely have an elevated stress field within the tensional dome within the shale and above the void. Comparing the line 5 and

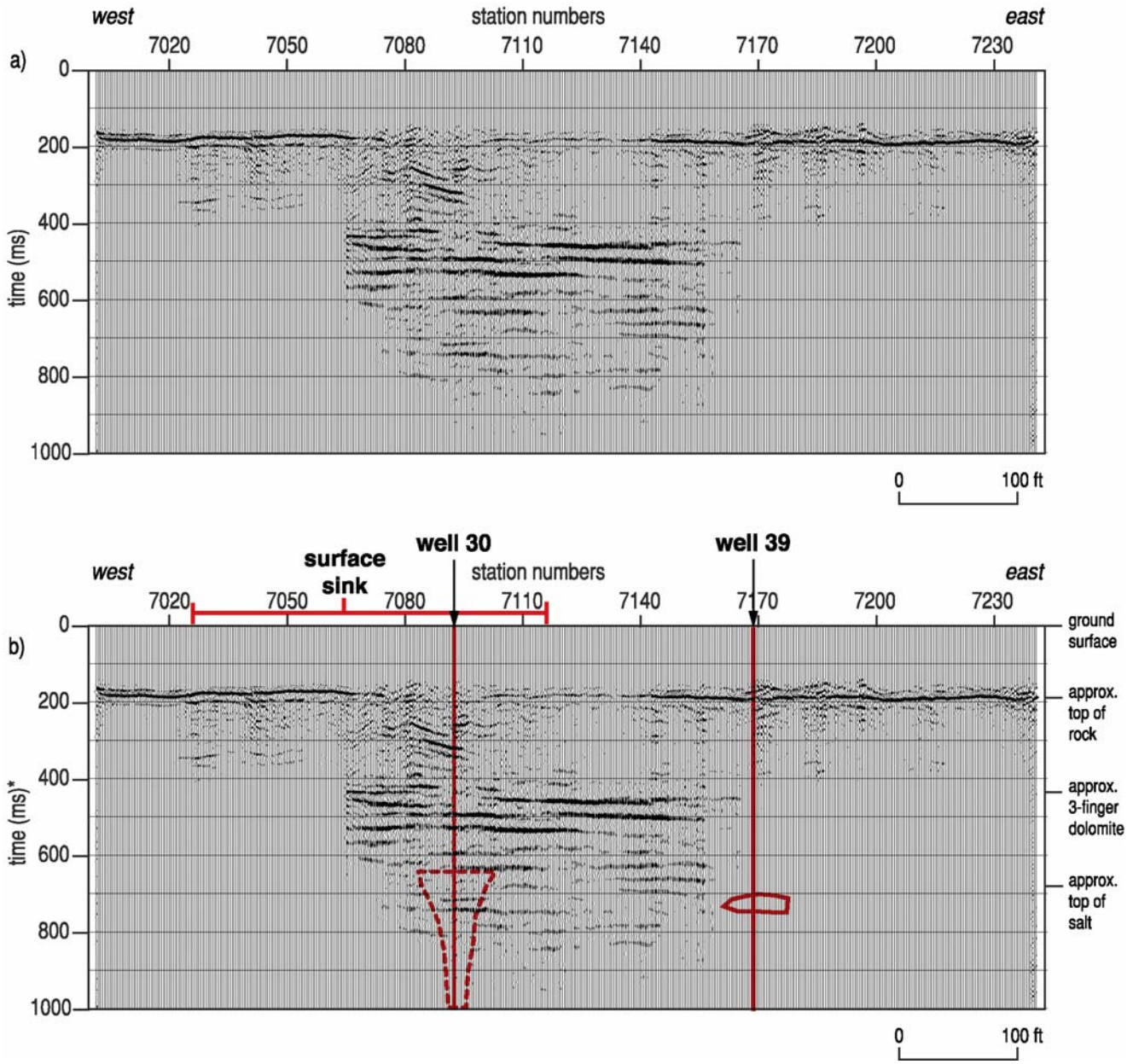


Figure 36. (a) W-E oriented CMP stacked section from line 7, acquired north of Carey Boulevard and adjacent to the metal building located on the east side of the property. Well #30 is approximately located at station 7092. Structural failure has already occurred at this well location, which coincides with a loss of reflection coherency and decreased stacking velocities, further strengthening this method as an indicator of relative stress changes in the subsurface. (b) Approximate cross section of salt jugs beneath well #39 as measured with recent sonar and well #30 estimated from historical data. Between station 7025 and 7115 the ground has subsided due to collapse of the jug at well #30. The relative positions of the wells and cavern sonar surveys superimposed on the seismic section were based on relative approximate locations, shapes, and depths, not interpreted from seismic results. Superimposition was performed by Burns & McDonnell. Dashed geometry and size of jug beneath well is approximately based on tonnage removed and historical borehole data while solid lines are derived from modern sonar, modern geophysical logs, tonnage, and historical borehole data. Well #30 is on the line at approximately station 7095 and well #39 is 26 ft south of the line at station 7169.

*See Figure 4 for approximate depth correlations.

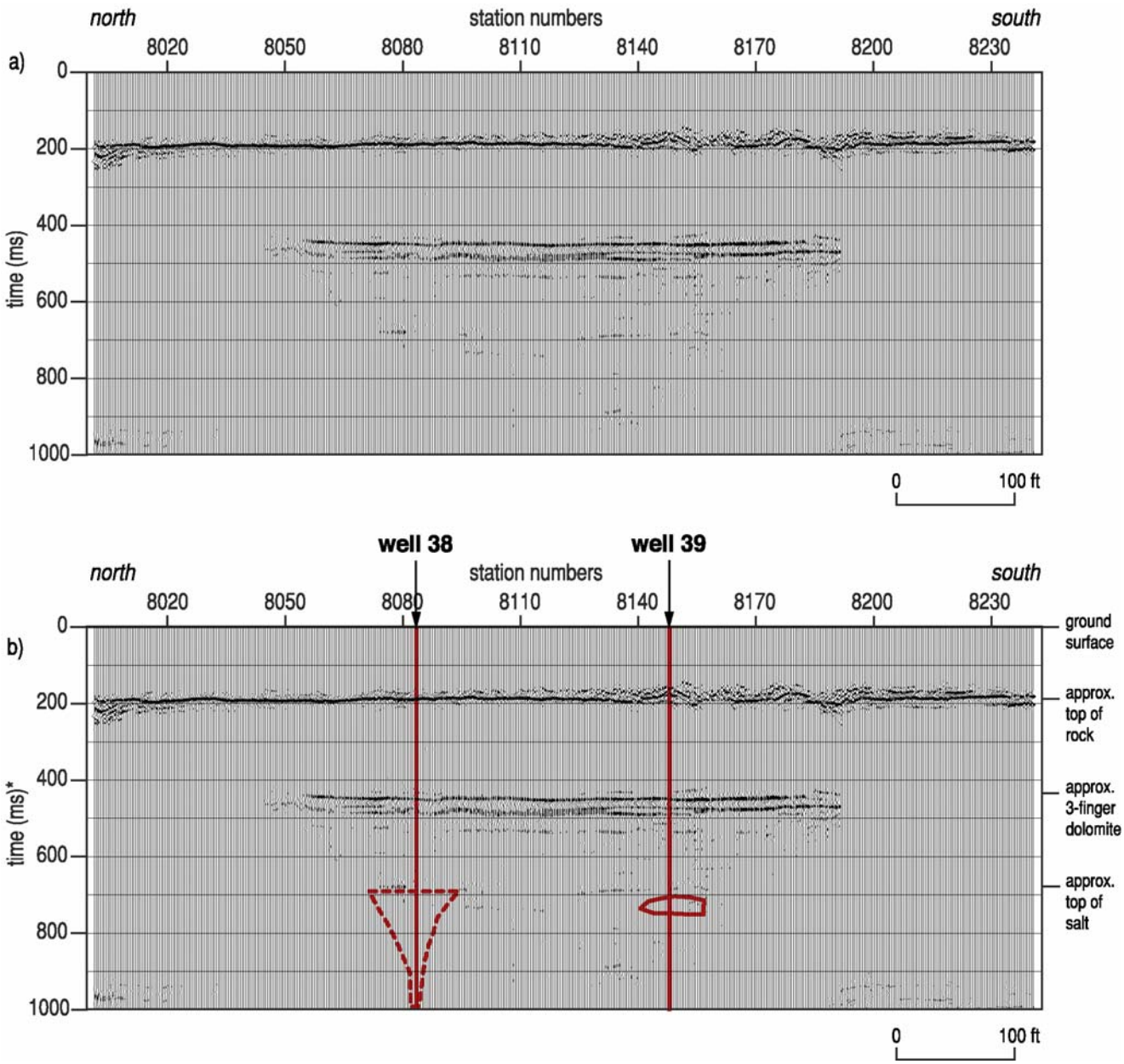


Figure 37. (a) N-S oriented CMP stacked section from line 8. The disturbed bedrock reflection between 8140 and 8200 is the result of crossing the gravel road, paved road, and railroad tracks. The dolomite reflection is evident at 450 ms, but only a subtle hint of the salt reflection can be seen at around 650 ms two-way travel time. (b) Approximate cross section of salt jugs seismic section estimated from recent sonar in well #39 and from historical data for well #38. The relative positions of the wells and cavern sonar surveys superimposed on the seismic section were based on relative approximate locations, shapes, and depths, not interpreted from seismic results. Superimposition was performed by Burns & McDonnell. Dashed geometry and size of jug beneath well is approximately based on tonnage removed and historical borehole data while solid lines are derived from modern sonar, modern geophysical logs, tonnage, and historical borehole data. Well #38 is located on the line at station 8083 and well #39 is located 10 ft west of station 8149.

*See Figure 4 for approximate depth correlations.

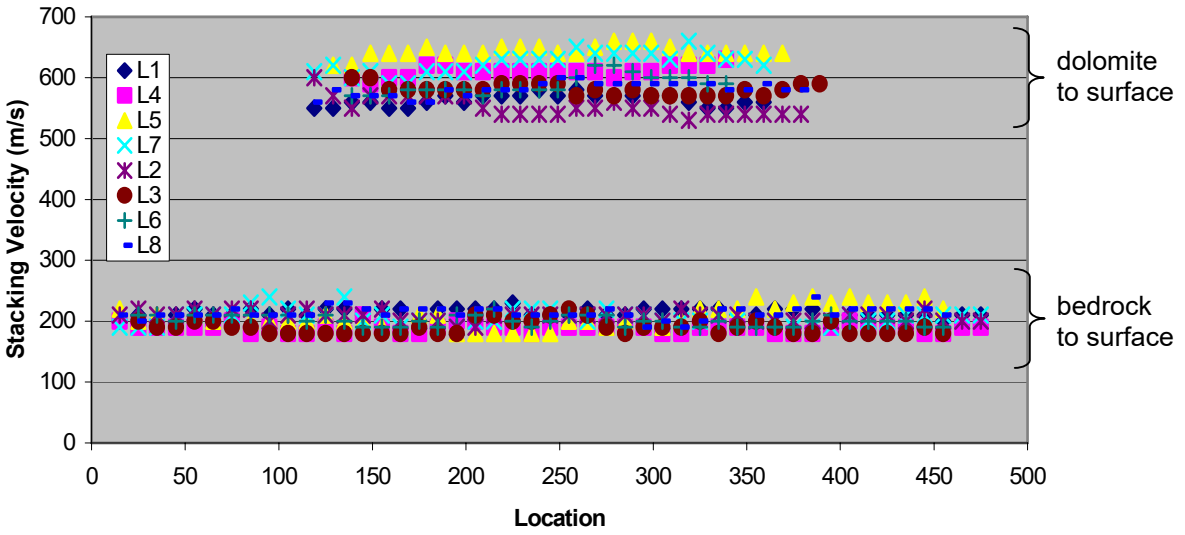


Figure 38. Stacking velocities for the bedrock and dolomite reflections are displayed for all eight seismic lines. Alluvium velocities are relatively consistent from line to line; however, larger variations are evident along the dolomite reflection. Line 1 exhibits lower velocities overall while line 5 has the highest velocities. Increased velocity between locations 275-300 on line 5 corresponds to well #25. Decreased velocities between locations 130-175 coincide with well #52 on line 4, with velocity increasing towards well #53 at location 322. Line 7 exhibits a lower relative velocity between locations 150-190, which is in agreement with known failure at well #30.

line 1 dolomite-reflection NMO velocities reveals a greater than 20% increase in shear velocity associated with line 5. From the loose theoretical development previously provided, this observation is consistent with the suggestion that rocks over an upward migration void are under elevated stress levels.

In general the scatter in the shear-wave velocity measurement is minimal with line 1 clearly possessing the lowest overall shear velocity and line 5 the highest (Figure 38). Line 4 and line 7 both have slightly higher shear velocities with line 7 slightly higher than the average on line 4. Considering line locations were not always optimal for investigating the target wells, looking at each profile individually in comparison to the well each profile crossed provides some interesting observations. Line 4 has two wells that could affect the shear-wave velocity, wells #52 and #53. Well #52 is coincident with a drop in NMO velocity, decrease in reflection coherency, and a decrease in shear-wave velocity and reflection coherency on the bedrock. This could be an indication of previous collapse that involved a void without sufficient volume to result in sinkhole formation. At the well #53 location there is an obvious increase in shear velocity, much like that observed on line 5. This phenomenon is considered consistent with a void large enough to elevate roof stress, such as the one imaged on sonar data from well #53.

Other isolated velocity maxima or minima that can be explained by surface observations, borehole examinations, or supposition are present on lines 4, 5, and 7. Besides the overall higher shear velocity on line 5, there is also a localized maximum apparently related to well #25 that exceeds the average along line 5. This localized, elevated shear velocity could be an indicator of possibly the highest stress observed above any wells targeted by this study. On line 7 both wells #30 and #39 are along the profile. The overall velocity is slightly higher along this line, which is likely related to the void imaged on 1993 compressional-wave seismic-reflection data and drill-confirmed. Line 7 also has a pronounced sinkhole that clearly indicates that voids in this part of

the site do have a history of migrating to the ground surface. Therefore, elevated shear velocity would not be considered completely out of character. The sinkhole along line 7 is coincident with a zone of decreased shear velocity associated with well #30. All the physical evidence to this point is consistent with theory, the assertions made based on the elastic modulus and all empirical data.

Isolating and describing changes in reflection character at locations with borehole-interrogated void provides fodder for hypothesizing about possible relationships between seismic-reflection signal and physical properties unique to conditions observed in these salt jugs. Diffraction-looking events can be interpreted near well locations on lines 3, 4, and 6. These diffraction events all have very similar slope with an apex at or near the dolomite reflection along lines 3 (3120), 4 (4140), and 6 (6110). The diffraction event on line 7 has an apex near station 7080 that originates at the bedrock surface and is coincident with the sinkhole at well #30. Diffractions are related to scatter points, which can be bed terminations (fault), abrupt discontinuities (erosional bed truncation), or point anomalies (rocks or boulders). The diffraction-looking events at 6110 are adjacent to a dropout-looking feature in dolomite reflection centered at 6125. This diffraction event at 6125 is directly over an extremely unusual-looking undulation in the salt reflection between 6110 and 6140. One final observation is the distinctive offset in dolomite reflection beneath station 5160. This is offset generally consistent with and slightly off-line from well #40.

***Surface-Wave Inversion***

Surface waves traditionally have been viewed as noise in multi-channel seismic data collected to image targets for shallow engineering, environmental, and ground-water purposes (Steeples and Miller, 1990). Recent advances in the use of surface waves for near-surface imaging have combined spectral-analysis techniques (SASW) developed for civil engineering applications (Nazarian et al., 1983) with multi-trace reflection technologies developed for near-surface (Schepers, 1975) and petroleum applications (Glover, 1959). The combination of these two uniquely different approaches to seismic imaging of the shallow subsurface permits non-invasive estimation of shear-wave velocities (within 15% of measured in many cases) (Xia et al., 2002) and delineation of horizontal and vertical variations in near-surface material properties based on changes in these velocities (MASW) (Park et al., 1996; Xia et al., 1999; Park et al., 1999).

Extending this imaging technology to include lateral variations in lithology as well as tunnel and fracture detection, bedrock mapping, and subsidence/karst delineation has required a unique approach that incorporates SASW, MASW, and CDP methods. By integrating these techniques, 2-D continuous shear-wave velocity profiles of the subsurface can be generated. Estimating the dispersion curve from up to 60 closely spaced receiving channels calculated every 3 ft to 6 ft along the ground surface enhances the signal and results in a unique, relatively continuous view of shallow subsurface shear-wave velocity properties. This highly redundant surface-wave method improves the accuracy of calculated shear-wave velocities and minimizes the likelihood that irregularities resulting from erratic dispersion curves will corrupt the analysis.

Surface-wave tests were performed along lines 1 and 4 (Figure 17). The intent of this testing was to determine what was necessary to record low-frequency surface waves that sufficiently sampled the bedrock to detect any build-up in stress along the bedrock surface. Localized increase in stress along the bedrock surface could be an indicator of an elevated collapse potential. Both lines were acquired in a consistent fashion using a standard MASW approach and

equipment. Unlike shear-wave reflection data, surface-wave data are depth limited by the frequency range of the source pulse. Unfortunately, the material characteristics at this site make producing frequencies below 10 Hz difficult and ultimately that limitation hindered sampling the stress field on the bedrock surface.

***Data Acquisition***

Two lines of MASW data with 15-ft source spacing were acquired using an accelerated weight drop (Figure 39) and a 144-channel Geometrics Geode seismograph (Figure 40) controlled by a rugged PC on a mobile platform (Figure 41). Line 1 runs east and west near the cemetery on the east end of the site, and line 4 runs north and south near the west property, south of Carey Boulevard. A fixed-spread geometry was used to acquire data on each line using a fixed 144-station spread with 4.5-Hz compressional receivers separated by 6 ft. Three consecutive shots were recorded separately at every station accessible to the source. Data were acquired between passing cars and trains when noise was minimal.

Figure 39. Accelerated weight drop, custom built at the KGS.

Figure 40. 144-channel Geometrics Geode seismograph.

Figure 41. Mobile PC platform used in recording surface-wave data.

***Data Processing***

Data from each source station were corrected for shot-to-shot variation in recording time and were vertically stacked. A representative shot gather (Figure 42) was selected from each line to test for the offset and spread length that produced the optimal dispersion curve with sufficient resolution of the fundamental mode and bandwidth (Figures 43 and 44). The offset and spread lengths for line 1 were 20 and 140 ft, respectively, and 20 and 200 ft for line 4. The larger spread length used for line 4 was selected for increased resolution of the fundamental mode on dispersion curves with interference from a higher-order mode (Figure 45). The 1-D shear-velocity profile was calculated for each dispersion curve using the SurfSeis© inversion algorithm; each profile was

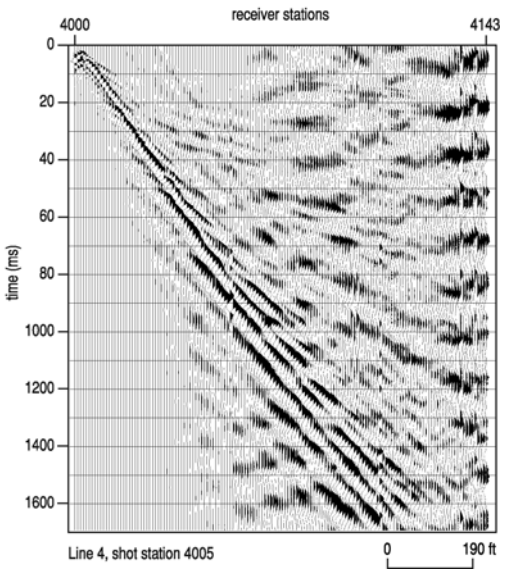


Figure 42. Surface-wave shot gather acquired along line 4. Weight-drop source produced distinguishable surface waves over 600 ft from the source with dominant frequencies as low as 10 Hz.

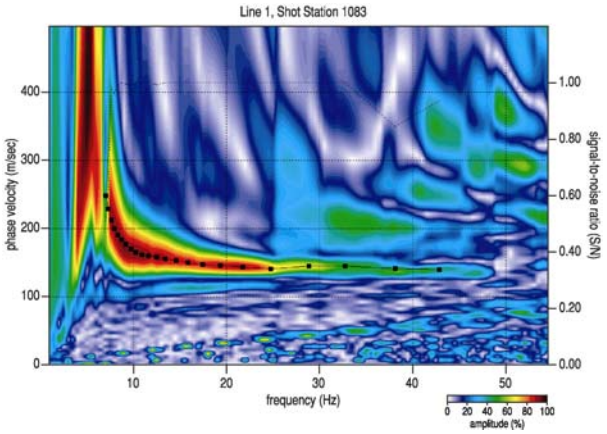


Figure 43. Representative dispersion curve from line 1. Color display is relative amplitude.

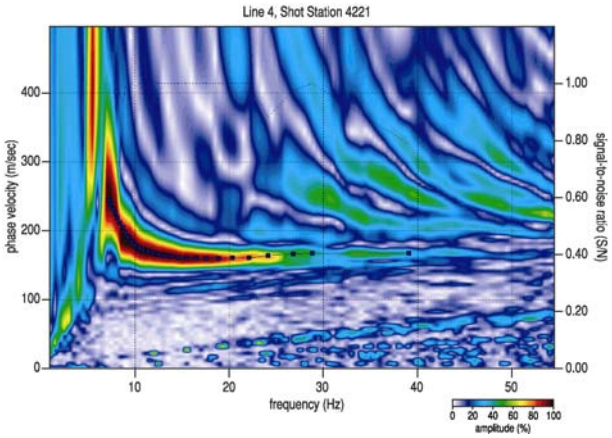


Figure 44. Representative dispersion curve from line 4. Overtone analysis allows confident picks on dispersion curve to frequencies as low as 8 Hz.

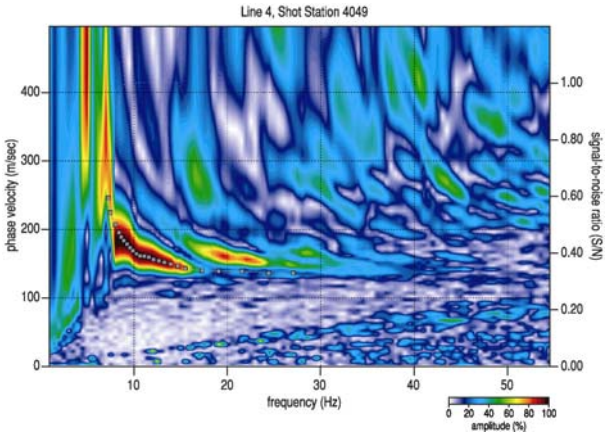


Figure 45. Overtone analysis from line 4 with uncharacteristic narrow frequency-band response evident in dispersion curve. Useable frequency band ranges from about 8 Hz to maybe as high as 25 Hz. A higher-order mode interferes with the fundamental mode beginning at 18 Hz.

associated with the receiver station in the middle of the selected spread. The 1-D profiles were assembled to create a 2-D profile for each line.

***Results***

The top of the bedrock is about 75 ft deep. The average shear velocity is about 1000 ft/s. Because the lowest frequency of recorded data is approximately 7 Hz, the deepest that surface waves can image is about 65 ft, just above the top of the bedrock. Data from line 1 produced a 2-D $V_s$ profile indicating approximately homogeneous horizontal layers that accurately reflect local geology (Figure 46). Data from line 4 produced a similar profile, with a velocity anomaly above the bedrock between station locations 4075 and 4125 (Figure 47). These CMP locations correspond exactly to the dispersion curves with interference from higher-order modes. A disturbance in the bedrock reflection on seismic shear-wave reflection data from the same line is located near the station locations of the anomaly in the MASW data (Figure 48).

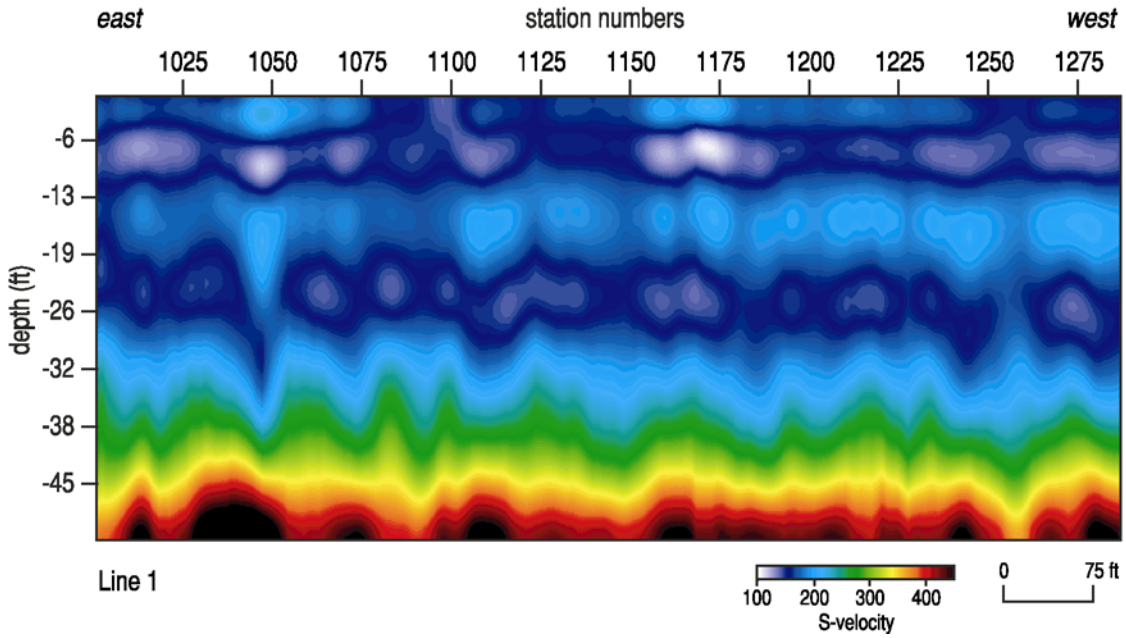


Figure 46. 2-D representation of shear-wave velocity field along line 1. From 30 ft to ground surface, the shear-wave velocity is relatively constant.

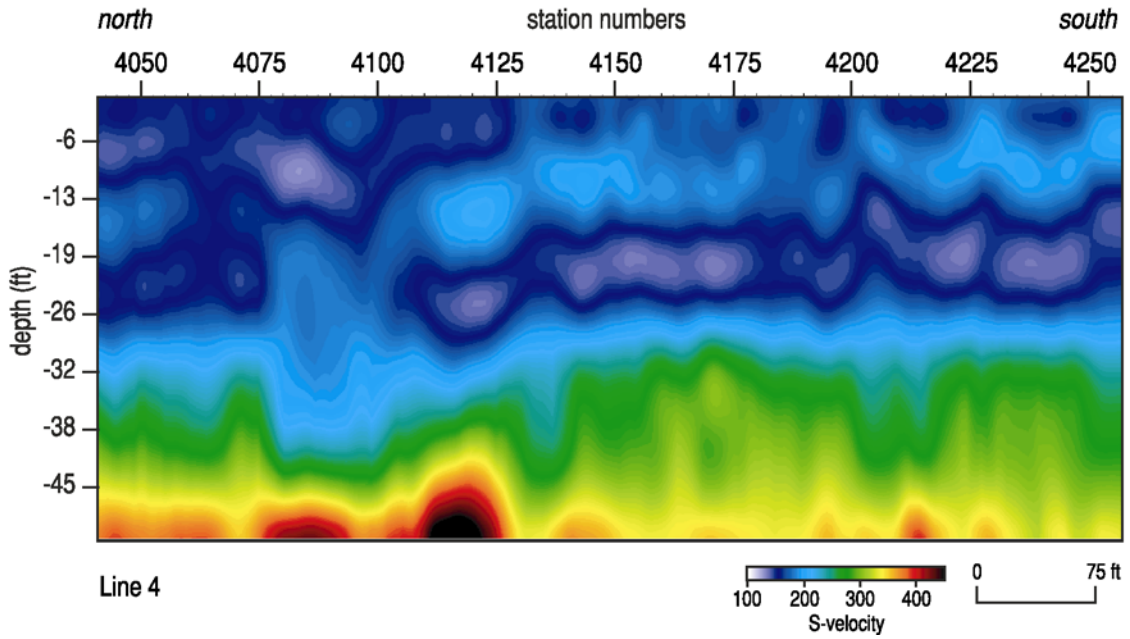


Figure 47. 2-D shear-wave velocity profile along line 4. Variability beneath station 4100 at around 40 ft below ground surface is consistent with a bedrock anomaly observed on the shear-wave reflection section.

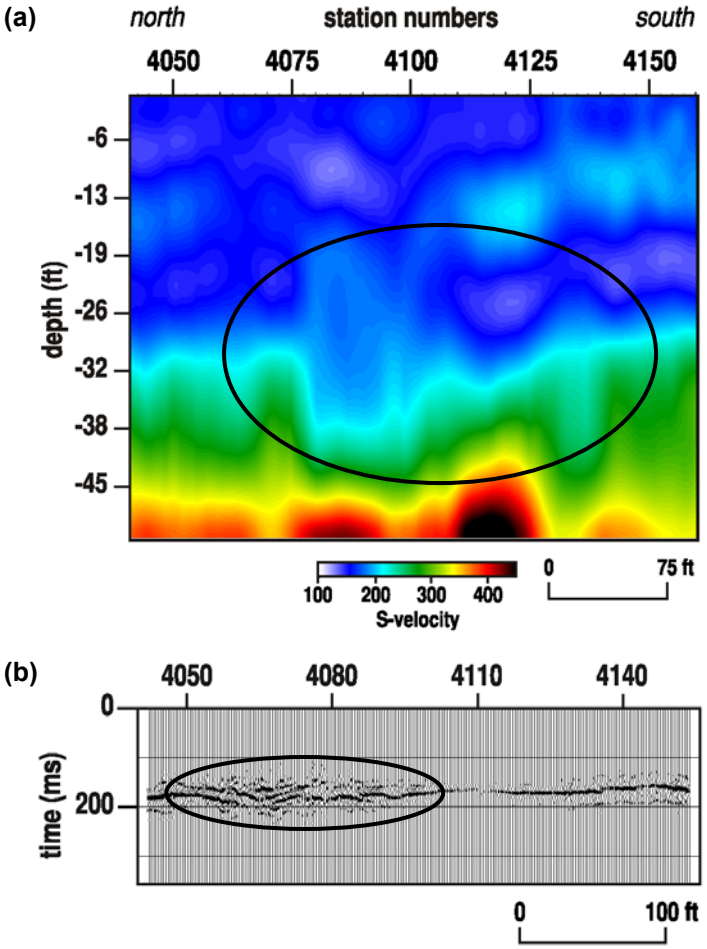


Figure 48. A low-velocity anomaly in the overburden (a) exists near the stations that correspond to a disturbance in the bedrock reflection in line 4 (b).

### *QA/QC*

The data acquired and processed on this survey were designed to allow the highest quality and most accurate acoustic representation of the geologic setting possible, given the project constraints. Current state-of-the-art techniques were used in a fashion that was appropriate and verified with step-by-step QA/QC. The most important (possibly even essential) information provided in this report (besides the CDP stacked section itself) is data in shot-gather format. This information allows the geophysicist and geologist to make determinations as to the accuracy and to some degree the authenticity of processed seismic sections and associated velocity analysis. Seismic-processing software and techniques are very powerful tools that, if not used properly, can and most likely will result in false interpretations.

The equipment and recorded data were continuously monitored during acquisition to allow production of the highest quality CMP stacked section. The response amplitude of receivers was monitored using a modified tap test performed after the planting of each geophone or group of geophones. The continuity and leakage of each active station was meter monitored prior to each shot. The system was subject to a series of pre-acquisition tests designed to ensure the integrity of analog filters, consistency in system noise, and precision in digitally stored data. Visual analysis of general signal-to-noise ratio, environmental noise, DC bias, and variations in the optimum recording window was performed frequently throughout the surveys.

## Discussion

Lateral variability in the velocity gradient can theoretically be related to changes in the stress field as defined by principles governing the elastic moduli in rocks. Reflection data from this study are the first to provide empirical evidence that the changes in stress related to the tensional dome concept of (Davies, 1951) can be non-invasively measured for underground caverns using shear-wave seismic reflection. For shear-wave seismic reflection to be a viable method to characterize the degree of change in stress associated with a single cavern at this site, resolution must be improved and velocity-discrimination techniques must be developed that can isolate changes in shear velocity at sub-spread distances.

These reflection data provide some of the most conclusive evidence for direct detection of salt jugs from surface geophysics. In several locations around this site, the reflection character changes abnormally when jugs are known to exist in the subsurface. These changes in reflection character are likely diagnostic of changes in rock properties or layer geometry related to voids. Diffraction-looking events seem to be present when voids migrate above the salt/shale contact, and on these data those diffractions are most notable at the dolomite layer. This is likely an indication that the salt jug has migrated to near the top of the upper Wellington Formation.

Surface-wave analysis showed great promise and is consistent with reflection interpretations within the unconsolidated portion of the section. Without recording surface waves that have a half wavelength equal to the depth of bedrock, the true potential of the method as an early warning system cannot be determined. If reduced shear-wave velocity can be detected on the bedrock system, then surface interests can be alerted to impending surface collapse and proper precautions put in place. The potential of surface-wave analysis of the bedrock surface is immense and represents a potentially excellent tool for assessing conditions that are conducive to sinkhole formation before bedrock failure.

**Recommendations**

Further study at this site could provide additional data necessary to extend and refine this research effort sufficiently to determine if

(a) the full potential of surface-wave monitoring can be actualized and if this site is a good candidate for long-term passive monitoring of the bedrock surface using surface waves; and
(b) a site-wide seismic characterization and monitoring program can be developed with clearly defined seismic target criteria and the associated tailored seismic methodology.

If this research were to be carried forward, the next round of experiments would be intended to validate the use of passive MASW monitoring along the railroad using the train noise as the energy source. Also necessary are methods for improving the resolution potential of NMO velocity assignments and design of low-cost 3-D approaches for imaging these extreme geometries. Ideally, anomalies identified as indicative of vertically migrating voids on CMP stacked sections can be drill investigated. Improving the penetration of this shear-wave reflection approach could provide focused images of the larger jugs at this site. Correlating drill and seismic data would provide the necessary confidence and guidance for continued development and design of follow-up shear-wave reflection surveys at selected locations across the site.

A site of this type provides unique research opportunities for the development of non-invasive geophysics approaches for characterizing 'deep' voids. If a long-term access agreement could be formulated to allow continued use of this site as a physical model, this research path appears to be leading to dramatic advancements in the science of void detection and quantification of potential collapse characteristics. Research along the lines proposed here would greatly benefit future efforts to delineate the migration potential of salt jugs throughout this part of Kansas as well as other places around the world where legacy dissolution mining of salt has left collapse-prone areas. Developments and unique findings that are possible at this site may be able to lead to much-needed constraints and rules of thumb for delineating and characterizing a variety of underground mines throughout the world.



Students from the University of Kansas and University of Leoben helped acquire, process, and interpret data in this report.

## Appendix

### Well Offsets from KGS Seismic Lines

| Line | Well | Station | Offset (m) | Offset (ft) | Direction |
|---|---|---|---|---|---|
| 1 | 87 | 1083 | | 0 | S |
| 1 | 88 | 1170 | | 0 | S |
| 1 | 89 | 1274 | | 0 | S |
| 2 | 86 | 2007 | 5 | 16.4 | E |
| 2 | 85 | 2131 | 5 | 16.4 | E |
| 2 | 99 | 2223 | 5 | 16.4 | E |
| 3 | 54 | 3091 | | 0 | S |
| 3 | 55 | 3187 | | 0 | N |
| 3 | 96 | 3287 | 27 | 88.56 | E |
| 4 | 53 | 4161 | | 0 | E |
| 4 | 59 | 4273 | 2 | 6.56 | W |
| 4 | 52 | 4070 | | 0 | W |
| 5 | 26 | n/a | 25 | 82 | N |
| 5 | 33 | n/a | 25 | 82 | N |
| 5 | 36 | n/a | 16 | 52.48 | N of east projection |
| 5 | 20 | 5035 | 2 | 6.56 | N |
| 5 | 40 | 5183 | 5 | 16.4 | S |
| 6 | 43 | 6069 | | 0 | E |
| 6 | 21 | 6117 | | 0 | E |
| 7 | 92 | 7269 (?) | 0 | 0 | n/a |
| 7 | 39 | 7169 | 8 | 26.24 | S |
| 7 | 29 | 7015 | 10 | 32.8 | S |
| 7 | 41 | 7049 | 20 | 65.6 | N |
| 8 | 38 | 8083 | 0 | 0 | n/a |
| 8 | 37 | 8015 | 0 | 0 | n/a |
| 8 | 39 | 8149 | 3 | 9.84 | W |

**References**


Coyner, K.B., 1984, Effects of stress, pore pressure, and pore fluids on bulk strain, velocity, and permeability in rocks: Ph.D. Dissertation. Cambridge, MA: Massachusetts Institute of Technology.

Davies, W.E., 1951, Mechanics of cavern breakdown: *National Speleological Society*, v. 13, p. 6-43.

Dellwig, L.F., 1963, Environment and mechanics of deposition of the Permian Hutchinson Salt Member of the Wellington shale: Symposium on Salt, Northern Ohio Geological Society, p. 74-85.

Dvorkin, J., A. Nur, and C. Chaika, 1996, Stress sensitivity of sandstones: *Geophysics*, v. 61, p. 444.

Glover, R.H., 1959, Techniques used in interpreting seismic data in Kansas: In Symposium on Geophysics in Kansas, ed. W.W. Hambleton. Kansas Geological Survey Bulletin 137, p. 225-240.

Hardage, B.A., 1983, *Vertical seismic profiling, Part A–Principles*: Geophysical Press.

Holdoway, K.A. 1978, Deposition of evaporites and red beds of the Nippewalla Group, Permian, western Kansas: Kansas Geological Survey Bulletin 215.

Khaksar, A., C.M. Griffiths, and C. McCann, 1999, Compressional- and shear-wave velocities as a function of confining stress in dry sandstones: *Geophysical Prospecting*, v. 47, n. 4, p. 487-508.

Kulstad, R.O., 1959, Thickness and salt percentage of the Hutchinson salt; in, Symposium on Geophysics in Kansas: Kansas Geological Survey Bulletin 137, p. 241-247.

Landes, K.K., and T.B. Piper, 1972, Effect upon environment of brine cavity subsidence at Grosse Ile, Michigan, 1971: Solution Mining Research Institute and BASF Wyandotte Corp.

Merriam, D.F., 1963, The Geologic History of Kansas: Kansas Geological Survey Bulletin 162, 317 p.

Merriam, D.F., and C.J. Mann, 1957, Sinkholes and related geologic features in Kansas: *Transactions of the Kansas Academy of Science*, v. 60, p. 207-243.

McGuire, D., and B. Miller, 1989, The utility of single-point seismic data: In Geophysics in Kansas, D.W. Steeples, ed.: Kansas Geological Survey Bulletin 226, p. 1-8.

Miller, R.D., D.W. Steeples, L. Schulte, and J. Davenport, 1993, Shallow seismic-reflection feasibility study of the salt dissolution well field at North American Salt Company's Hutchinson, Kansas, facility: *Mining Engineering,* October, p. 1291-1296.

Nazarian, S., K.H. Stokoe II, and W.R. Hudson, 1983, Use of spectral analysis of surface waves method for determination of moduli and thicknesses of pavement systems: Transportation Research Record No. 930, p. 38-45.

Park, C.B., R.D. Miller, D.W. Steeples, and R.A. Black, 1996, Swept impact seismic technique (SIST): *Geophysics*, v. 61, p. 1789-1803.

Park, C.B. R.D. Miller, and J. Xia, 1999, Multichannel analysis of surface waves (MASW): *Geophysics*, v. 64, p. 800-808.

Schepers, R., 1975, A seismic reflection method for solving engineering problems: *Journal of Geophysics*, v. 41, p. 267-284.

Steeples, D.W., and R.D. Miller, 1990, Seismic reflection methods applied to engineering, environmental, and groundwater problems: In *Volume I: Review and Tutorial*, S.H. Ward, ed.: Society of Exploration Geophys, Investigations in Geophysics no. 5, p. 1-30.

Swineford, A., 1955, Petrography of upper Permian rocks in south-central Kansas: State Geological Survey of Kansas Bulletin 111, 179 p.
Walters, R.F., 1978, Land subsidence in central Kansas related to salt dissolution: Kansas Geological Survey Bulletin 214, 82 p.
Whittemore, D.O., 1990, Geochemical identification of saltwater contamination at the Siefkes subsidence site: Report for the Kansas Corporation Commission.
Whittemore, D.O., 1989, Geochemical characterization of saltwater contamination in the Macksville sink and adjacent aquifer: Kansas Geological Survey Open-file Report 89-35.
Winkler, K.W., 2005, Borehole damage indicator from stress-induced velocity variations: *Geophysics*, v. 70, n. 1, p. F11-F16.
Xia, J., R.D. Miller, and C.B. Park, 1999, Estimation of near-surface shear-wave velocity by inversion of Rayleigh waves: *Geophysics*, v. 64, n. 3, p. 691-700.
Xia, J., R.D. Miller, C.B. Park, J.A. Hunter, J.B. Harris, and J. Ivanov, 2002, Comparing shear-wave velocity profiles from multichannel analysis of surface wave with borehole measurements: *Soil Dynamics and Earthquake Engineering*, v. 22, n. 3, p. 181-190.